https://doi.org/10.1070/RCR5001

Photopharmacological compounds based on azobenzenes and azoheteroarenes: principles of molecular design, molecular modelling, and synthesis

Mikhail N. Ryazantsev,[a, b]* Daniil M. Strashkov,[a] Dmitrii M. Nikolaev,[a] Andrey A. Shtyrov,[b] Maxim S. Panov [b]

[a] *Institute of Biomedical Systems and Biotechnology, Peter the Great St. Petersburg Polytechnic University,*
Polytechnicheskaya ul. 29, 195251 Saint Petersburg, Russian Federation
[b] *Institute of Chemistry, Saint Petersburg State University,*
Universitetskii prosp. 26, 198054 Saint Petersburg, Russian Federation

Photopharmacology is a field of medicine and pharmacology that uses light to selectively activate or deactivate pharmaceutical agents. This approach significantly enhances and localizes the drug action and, therefore, reduces its side effects. Apart from the bioactive moiety, any photopharmacological compound should contain a photoactive group that must absorb light at the desired wavelength and reorganize the molecular structure after photoactivation. The design of an effective photopharmacological compound requires careful tuning of physical, chemical, and biological properties. The present review summarizes and analyzes the main approaches to the molecular design of photopharmacological drugs based on azobenzene or azoheteroarenes. The main ideas and methods used for tuning spectral and photochemical properties of compounds of this class are discussed. A comparative analysis of main computational methods for their *in silico* screening is carried out; the most common approaches to the synthesis of azobenzenes and azoheteroarenes derivatives are systematized. Special attention is given to the methods and approaches that are specific to the molecular design of photopharmacological compounds with required physicochemical and photochemical properties.
The bibliography includes 212 references.

Contents

1. Introduction 869
2. Specific features of molecular design of photopharmacological compounds in comparison with regular drugs 869
3. Specific features of molecular design of photoswiches for photopharmacological applications in comparison with photoswitches for other fields 870
4. Spectral, photochemical and acid – base properties of azobenzene 870
5. Main approaches to the design of azobenzene derivatives with optimal properties for photopharmacological applications 872
   5.1. Optimization of spectral properties 872
      5.1.1. Introduction of electron-donating and electron-withdrawing substituents into azobenzene 872
      5.1.2. Azoheteroarenes 873
      5.1.3. Protonation of the azo group nitrogen atoms. Azonium cations 874
      5.1.4. Protonation of other heteroatoms 875
      5.1.5. Steric effect of substituents in isomers. Bridged azobenzenes (dihydrobenzodiazocines) 875
      5.1.6. Electronic effect of substituents in isomers 876
   5.2. Optimization of properties required for the stability of a photopharmacological drug *in vivo* 876
6. Key methods for the computational modelling used for the molecular design of photopharmacological drugs 877
   6.1. Modelling of the spectral properties of azobenzenes 877
   6.2. Modelling of relative energies of isomers and thermal isomerization of azobenzene derivatives 878
   6.3. Methods for estimating the ligand – receptor binding affinity 878
7. Main approaches to the synthesis of azobenzene- and azoheteroarene-based molecular switches 880
   7.1. Synthesis of azobenzene-based photoswitches 880
      7.1.1. Azo coupling reaction 880
      7.1.2. Mills reaction 881
      7.1.3. Oxidative coupling of anilines 881
      7.1.4. Reductive coupling of nitroarenes 882
      7.1.5. Coupling of arenediazonium salts with aryllithium derivatives 882

Received 25 August 2020
© 2021 Uspekhi Khimii, ZIOC RAS, Russian Academy of Sciences and IOP Publishing Limited

7.1.6. Coupling of arylhydrazines with aryl halides 882
7.1.7. Reaction of triazenes with phenols and anilines 883
7.1.8. Reaction of quinones with arylhydrazines 883
7.1.9. Miscellaneous reactions 883
7.2. Methods for the synthesis of bridged azobenzenes 883
7.2.1. Reductive intramolecular coupling of 1,2-bis(2-nitrophenyl)ethane derivatives 883
7.2.2. Mills reaction 883
7.3. Synthesis of azoheteroarenes 884
7.3.1. Azo coupling reaction 885
7.3.2. Mills reaction 886
7.3.3. Oxidative coupling of hetarylamines 886
7.3.4. Reactions of quinones with arylhydrazines 886
7.3.5. Coupling of arenediazonium salts with hetaryl lithium derivatives 887
7.3.6. Coupling of arylhydrazines with hetaryl halides with the subsequent oxidation 887
7.3.7. Heterocycle assembly 887
7.3.8. Miscallaneous methods for the synthesis of azoheteroarenes 888
8. Conclusion 888
9. List of acronyms and designations 889

1. Introduction

Photopharmacology [1–14] is a new rapidly evolving field of science at the intersection of physiology, medicine, and pharmacology, which uses drugs with light-regulated biological activity. Such light regulation increases the localization of drug action and decreases its negative side effects. Although nowadays such drugs are not yet used in clinical practice, researchers have demonstrated the possibility of photopharmacological control for a number of important biological objects in the cell, including G-proteins,[15–17] ionotropic receptors,[18–20] ion channels,[3,4,18] cytokines,[21] DNA, and RNA.[22] Experimental studies show the possibility of applying the concept of photopharmacology to design photocontrolled analgesic drugs,[23,24] photocontrolled antibiotics,[25] photohormones,[26] drugs for cancer photochemotherapy,[27] for the treatment of neurodegenerative disorders,[28] and for restoration of the visual function of the degenerated retina.[29,30] A change in the structure of a photopharmaceutical drug after light irradiation, which can be either reversible or irreversible, occurs, for example, in the presence of photoremovable protecting groups [31,32] or genetically encoded photoswitchable amino acids.[33] Most often, in the design of these drugs, fragments of molecular photoswitches, *i.e.* compounds which can be reversibly converted from one form to another upon photostimulation at specified wavelengths, are introduced into the molecule. To date, most of the proposed photopharmaceuticals include a photoswitchable azobenzene or azoheteroarene scaffold.

M.N.Ryazantsev. Doctor of Chemical Sciences, Associate Professor at the Department of Laser Chemistry and Laser Materials Science of the Institute of Chemistry, SPbU, Leading Researcher at the Laboratory of Nanobiotechnology of the Saint Petersburg Academic University.
E-mail: mikhail.n.ryazantsev@gmail.com
D.M.Strashkov. Postgraduate Student at SPbAU.
E-mail: danielstr@mail.ru
D.M.Nikolaev. Postgraduate Student at the same University.
E-mail: dmitrii.m.nikolaev@gmail.com
A.A.Shtyrov. Postgraduate Student at the same University.
E-mail: andriei.shtyrov@gmail.com
M.S.Panov. Researcher at the Institute of Chemistry of SPbU.
E-mail: m.s.panov@spbu.ru
Current research interests of the authors: investigation and development of photoactivated chemical and biological systems, development and application of computational methods for the study of chemical and biological systems and processes, photopharmacology.

The objective of the present review is to systematize and compile information on the molecular design and synthesis of photopharmacological drugs based on azobenzenes and azoheteroarenes. The data essential to have an insight into the synthesis of these compounds are presented. Classical approaches to the drug design are available in numerous reviews and monographs (see, *e.g.*, Refs 34–39). General description of properties of azobenzene and azoheteroarene switches and the examples of their practical application can be found in reviews.[40–44]

2. Specific features of molecular design of photopharmacological compounds in comparison with regular drugs

One of the modern concepts of pharmacology as a science of developing novel pharmaceutical drugs is based on the interaction between a biotarget (protein, DNA, or another biomolecule involved in the corresponding metabolic or signalling processes in the body) and a ligand. The ligand, which is considered to be a potential drug, must bind to the desired biotarget. The binding affinity between the ligand and the biotarget, along with other factors, determines the drug efficacy (maximum possible therapeutic effect) and activity, usually characterized by the value of EC_{50} (concentration which can induce a response equal to 50% of the maximum response). The absence of biological response towards other potential targets determines the drug selectivity.

However, the presence of biological activity is not the only requirement for the development of a potent drug. The design of a medicinal agent often imposes additional restrictions on the physicochemical and biochemical properties of a potential drug, which correlate with the pharmacokinetic characteristics. These properties include hydrophilicity and lipophilicity, resistance to biochemical processes occurring in the body, *etc.*

When developing photopharmaceutical drugs, the following factors should be taken into consideration.

1. The affinity of photopharmacological agents to a biological target should differ for the deactivated and activated forms. (Ideally, it should be equal to zero for the deactivated form).

2. For possible therapeutic use, photopharmacological drugs should absorb light in the range of optical transparency of biological tissues (in a wavelength range of 650–1450 nm).

3. When the photostationary equilibrium is established, the concentration of the active form of the drug (which is usually thermodynamically less stable) should be sufficient for the therapeutic effect. The photostationary equilibrium which can be achieved upon light irradiation at a specific wavelength is determined by quantum yields of the forward and reverse photoisomerization, the energy barrier of thermal transition from one form to the other, temperature, and the difference between the absorption coefficients of isomers at the given wavelength (Fig. 1). Therefore, an indispensable condition is a difference between the absorption spectra of different isomers at the working wavelength, *i.e.* either the band centres should be shifted relative to each other, or the intensity of the bands should be very different.

4. To localize the action of a photopharmacological drug, it is necessary that the active form (that is thermodynamically less stable) appears only after irradiation and that its concentration is optimal when thermodynamic equilibrium is reached. This condition places a restriction on the Gibbs energy difference between the *E*- and *Z*-forms of the drug.

5. Also, deactivation of the active drug form after a certain period of time is desirable so that to avoid the spread of the substance in its active state beyond the zone of therapeutic action. However, if the deactivation rate is too high, the desired concentration of the active form would not be achieved at the photostationary equilibrium. Therefore, it is necessary to find the optimal rate of thermal isomerization (reaction energy barrier) from the thermodynamically less stable form to the more stable form.

3. Specific features of molecular design of photoswiches for photopharmacological applications in comparison with photoswitches for other fields

Since photopharmacological agents are generally used in water-soluble media at physiological pH and they, most often, contain heteroatoms, the acid – base characteristics of the molecule are significant for drug development. The functional groups introduced to tune any biological, chemical, or physical properties can change the pK_a values of the acid – base groups present in the molecule and thereby alter all characteristics of the drug. As will be seen from the following analysis of examples of the design of potential photopharmacological drugs, this effect can not only be used to attain the desired characteristics but also become an obstacle to achieve required properties.

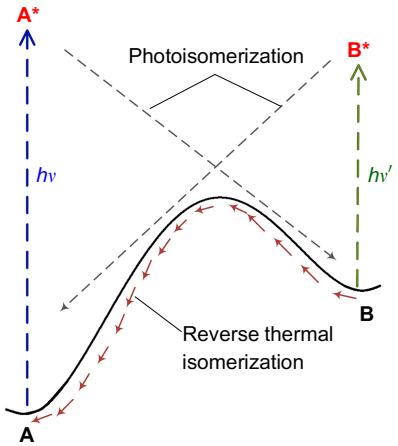


Figure 1. Scheme of a photocycle for a molecular photoswitch. **A**, **A*** and **B**, **B*** are the ground and excited states of the two forms of the photoswitch. Upon photon absorption, the switch is converted from the thermodynamically more stable form **A** to the thermodynamically less stable form **B**, activating the pharmacological agent bound to the molecular photoswitch. The reverse transition from the photoactivated active form B to the thermodynamically more stable inactive form A is performed *via* thermal isomerization or *via* photoactivated path.

The structure of proposed photoswitches is restricted by requirements to the size of molecules of potential pharmaceutical drugs (usually up to 500 atoms), their hydrophilicity and lipophilicity,[45] and the absence of toxicity. For example, it is not recommended to use bulky supramolecular complexes, compounds with a large number of benzene rings and extended hydrocarbon chains or those containing toxic metals as the scaffolds.

A photopharmacological drug must be stable to biochemical processes occurring *in vivo*. It is not always possible to predict the effect of the cellular environment on the stability of a drug, and often the problems can be identified only in the stage of the *in vivo* trials. However, certain properties of the compounds can be identified in advance. For azobenzene- and azoheteroarene-based drugs such properties include mainly resistance to hydrolysis and to the reduction by thiols contained in the body.

4. Spectral, photochemical and acid – base properties of azobenzene

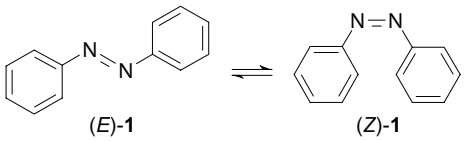
The physicochemical and spectral characteristics as well as the acid – base and kinetic properties of azobenzenes and azoheteroarenes are strongly influenced by the nature of substituents and heteroatoms contained in the molecular photoswitch. As a basic compound for design, it is convenient to choose azobenzene (**1**), the properties of which are well studied.[46 – 50]

The absorption spectrum of the *E*(*trans*)- and *Z*(*cis*)-isomers of compound **1** (Scheme 1; for explanation of the designations, see below) in ethanol exhibits two broad bands, the fitting of which to Gaussian functions (see below)[46] reveals the vibronic structure.

A low-intensity band was detected in the visible region corresponding to a series of electronic vibrational n → π* transitions [the wavelength corresponding to maximum light absorption: (λ_{max}) ≈ 443 nm for the *E*-isomer and ≈432 nm for the *Z*-isomer], while in the ultraviolet region more intense band appeared corresponding to a series of electronic vibrational π → π*-transitions (λ_{max} ≈ 320 and 281 nm for the *E*- and *Z*-isomers, respectively, Fig. 2).[47]

The frontier orbitals for *E*- and *Z*-azobenzenes are depicted in Fig. 3. The highest occupied molecular orbital

Scheme 1



(*E*)-**1** (*Z*)-**1**

ΔG = 10 – 12 kcal mol^{-1}

Isomer	λ_{max} (ππ*), nm (see [47])	λ(nπ*), nm (see [47])	Φ (λ_{ex}, nm)[50]
(*E*)-**1**	320	443	0.135 (313); 0.315 (436)
(*Z*)-**1**	281	432	0.328 (313); 0.469 (436)

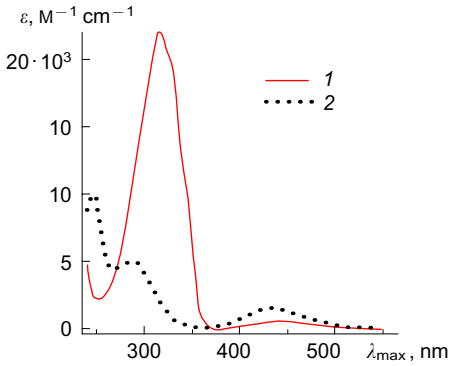


Figure 2. Absorption spectra of *E*- (*1*) and *Z*-forms (*2*) of azobenzene (**1**). The figure was composed by the authors using data of Ref. 49.

(HOMO) of azobenzene is a σ-orbital located on the azo nitrogen atoms. The HOMO-1 orbital, preceding in energy to the HOMO, and the lowest unoccupied molecular orbital (LUMO) are π-orbitals. The transition from the ground to the first excited singlet state $S_0 \rightarrow S_1$ (nπ*-transition) in (*E*)-azobenzene is symmetry-forbidden due to the planar geometry; it appears in the spectrum as a very weak band due to vibrational deformations. The intensity of $S_0 \rightarrow S_1$ (nπ*) transition for the *Z*-form is higher due to the deformation of the planar geometry. The $S_0 \rightarrow S_2$ (ππ*) transitions are much more intense than $S_0 \rightarrow S_1$ (nπ*) for both the *E*- and *Z*-isomers of azobenzene. In this case, the intensity of the $S_0 \rightarrow S_2$ (ππ*) transition for the *E*-form exceeds that for the similar transition of the *Z*-form.

One of the most detailed studies of the azobenzene spectrum was reported by Vetráková *et al.*[46] It was demonstrated that the spectrum of *Z*-azobenzene in ethanol can be approximated by three Gaussian functions with the following maxima [given in parentheses is the molar absorption coefficient (ε) in L mol^{-1} cm^{-1}]: 281.1 (5000), 425.2 (1050), and 453.4 nm (510); while the approximation of the absorption bands for the *E*-isomer requires six Gaussian functions with maxima at the following wavelengths: 280.5 (30 500), 304.3 (13 120), 324.0 (17 780), 332.6 (3530), 346.1 (5440), and 443.3 nm (460).[46]

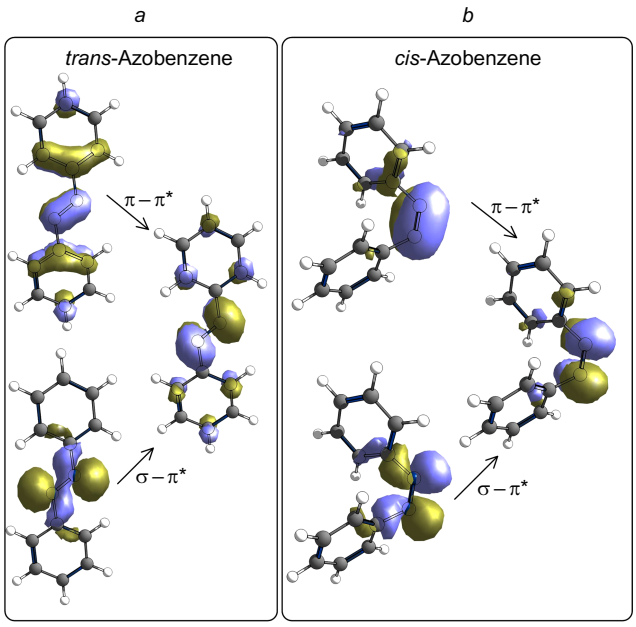


Figure 3. Electron transitions between HOMO, HOMO-1, and LUMO for *trans*- (*a*) and *cis*-isomers (*b*) of azobenzene.

The *E*-isomer of azobenzene is thermodynamically more stable than the *Z*-isomer [the Gibbs energy difference (ΔG) between the two forms of the molecular photoswitch is 10 – 12 kcal mol^{-1}]. In the dark (*E*)-azobenzene is virtually the only isomer (its content exceeds 99.99%).[48] It was shown that the quantum yield (Φ) of photoisomerization of both *E*- and *Z*-azobenzenes is higher upon excitation at the n → π* band than at the π → π* band: $\Phi_{E \rightarrow Z}$ (313 nm) = 0.130, $\Phi_{Z \rightarrow E}$ (313 nm) = 0.328; $\Phi_{E \rightarrow Z}$ (436 nm) = 0.315, $\Phi_{Z \rightarrow E}$ (436 nm) = 0.469; the measurements were performed in methanol at 25 °C.[50] The quantum yields depend on the excitation wavelength (given in parentheses), temperature, and viscosity of the solvent. It was demonstrated that after the optical transition of the *Z*- and *E*-isomers of azobenzene into the first excited state, deactivation proceeds through the conical intersection between two electronic states S_1/S_0 and can follow two pathways leading either to the isomerized product or back to the substrate.[43, 51] Deactivation of the second excited state proceeds in two steps. It includes the transition to the S_1 surface through the S_2/S_1 conical intersection and the subsequent transition to the S_0 surface *via* two possible pathways:

— through the S_1/S_0 conical intersection leading either to the product or to the substrate;

— through an alternative S_1/S_0^* conical intersection, which leads exclusively to the product.

Thus, the quantum yields of isomerization reactions upon the excitation of azobenzene to S_1 and S_2 states are different.

Z-form of azobenzene may be generated by photoactivating both n → π* and π → π* transitions. However, the following factor should be borne in mind when developing photopharmacological drugs: the n → π* band can be used for activation in the visible region, but the strong overlap of these bands for *Z*- and *E*-azobenzenes and low band intensity [ε_E (436 nm) = 486.2 ± 0.3 L mol^{-1} cm^{-1}; ε_Z (436 nm) = 1402 ± 23 L mol^{-1} cm^{-1}] precludes attaining the *Z*-isomer concentration required for physiological effect in the absence of an intense light source. The bands of the π → π* transition of the *Z*- and *E*-isomers are fairly well separated, and, besides, the band of the *E*-form is much more intense [ε_E (313 nm) = 22 337.4 ± 1.0 L mol^{-1} cm^{-1}; ε_Z (280 nm) = 4976 ± 59 L mol^{-1} cm^{-1}]. Thus, the desired concentration of the *Z*-form can be attained in the photostationary equilibrium. However, the π → π* bands are located in the UV region of the optical spectrum, which is unacceptable for photopharmacological applications because of the low permeability of biological tissues and its high toxicity. Fischer[52] showed that upon continuous irradiation at 313 and 436 nm, the relative photostationary concentrations of the *Z*-form (80 and 10%, respectively) are attained.

There are two known mechanisms of azobenzene thermal isomerization, involving

— a biradical transition state, in which the π-electron pair of the azo group double bond splits and each electron is located on one of the nitrogen atoms. The order of the N=N bond decreases and rotation about this bond becomes possible;

— a charge transfer transition state. In this case, the π-electron pair of the azo group double bond is located on one of the nitrogen atoms to form a lone pair, which results in an inversion at this atom.

The relative energy of the transition states can vary depending on the substituents and(or) the solvent. Isomerization can occur by either of these two mechanisms or by a mixed mechanism if both transition states have similar energies. Based on the results of computational modelling, the possibility of nonradiative transition from the ground to the triplet (T_1) state and isomerization *via* the triplet state was demonstrated.[53] However, this assumption has not been confirmed as yet.

Azobenzene is a very weak base ($pK_a^E = -2.6$, $pK_a^Z = -1.6$), and the spectrum of its protonated form can be obtained only in strongly acidic solutions.[54]

5. Main approaches to the design of azobenzene derivatives with optimal properties for photopharmacological applications

5.1. Optimization of spectral properties

For photopharmacological applications of molecular switches based on azobenzene derivatives, one should attain either bathochromic shift of the π → π* bands while retaining the difference in their intensities or better separation and increase in the intensities of the n → π* bands for the *Z*- and *E*-isomers. In practice, both approaches are employed.

The following main strategies for the shift of the π → π* transition band to longer wavelengths have been proposed:

— introducing electron-donating and electron-withdrawing substituents to the benzene rings;

— applying π-excessive or π-amphoteric azoheteroarenes, containing nitrogen or sulfur atoms;

— changing the pK_a values of the azo group nitrogen atoms *via* introducing substituents into the azobenzene scaffold and generation of the azonium cation at physiological pH;

— changing the pK_a values of heteroatoms other than the nitrogen atoms of the azo group.

To separate the bands of the n → π* transitions for the *Z*- and *E*-isomers so that to use these bands as working ones, two approaches are used.

1. Deformation of the planar geometry of azobenzene changes the energy of σ-orbitals of the azo group in the *E*- and *Z*-forms, contributing to the separation of the n → π* bands, and also increases the intensities of the n → π* bands. This approach has been implemented for the derivatives of dihydrobenzodiazocine, bridged azobenzene, and its hetero analogues.

2. Substitution at the *ortho*-position of the benzene ring relative to the azo group facilitates the separation of the n → π* absorption bands of the *E*- and *Z*-isomers due to electronic effects. In this case, it is necessary to achieve different effects of substituents on the energy of the azo group σ-orbitals in the *E*- and *Z*-isomers.

5.1.1. Introduction of electron-donating and electron-withdrawing substituents into azobenzene

The substituent effect on the shift of the π → π* bands of azobenzene is well studied; this effect is often used in the design of photoswitches (Figs 4, 5; Table 1, 2).[47, 55 – 67] For the development of photopharmacological drugs for clinical practice, it is important that the introduction of an electron-donating substituent into aromatic ring conjugated to the azo group shifts the π → π* band to longer wavelengths. The presence of the electron-withdrawing substituent in the other aromatic ring, also conjugated to the azo group, further enhances this effect. In the spectra of push-pull compounds, the red shift of the π → π* band to 400 – 470 nm can be observed.

Table 1. Positions of π → π* bands in the absorption spectra and lifetimes for the *Z*-isomer of monosubstituted azobenzenes ($RC_6H_4N{=}NC_6H_4$).

R	λ_{max}, nm	Solvent	$t_{1/2}$, h (*T*, °C) [a]	Ref.
H	320 (443) [b]	Ethanol	–	48
3-Me	322	Ethanol	–	48
4-F	323 (440)	Ethanol	–	48
3-NO_2	326	Ethanol	–	48
4-I	331 (445)	Ethanol	–	48
4-NO_2	338 (474)	Ethanol	–	48
4-OEt	348 (434)	Ethanol	–	56
4-NH_2	363	Cyclohexane	2 (35)	58
4-NMe_2	390	Cyclohexane	8.1 (25)	58
4-NEt_2	407	Cyclohexane	0.5 (25)	58

Note. Here and in Table 2 the dash indicates that no data are available.
[a] The lifetime (the halflife period) of the unstable *Z*-isomer; [b] Wavelength of the π – π* transition (in parentheses, n – π* transition wavelength).

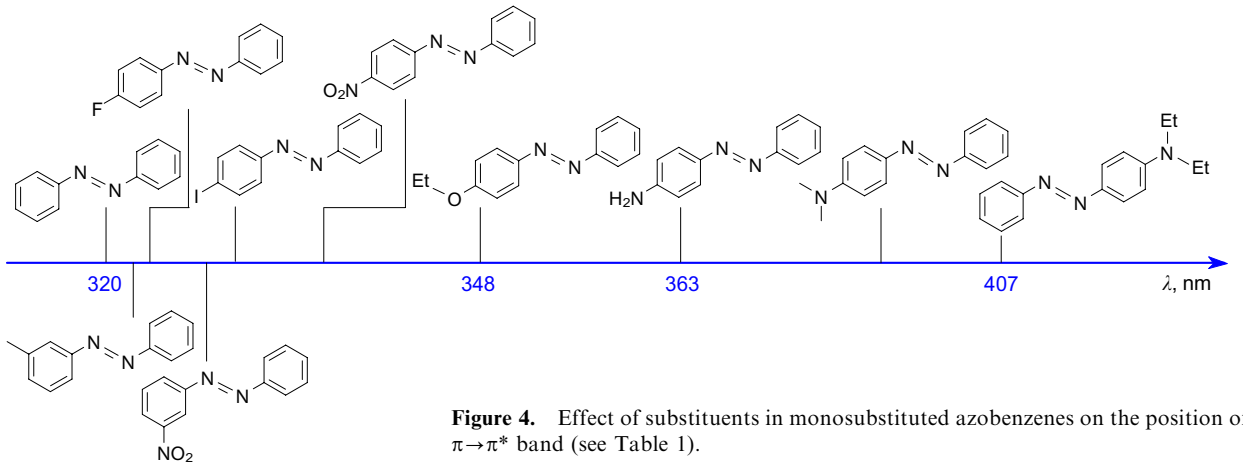


Figure 4. Effect of substituents in monosubstituted azobenzenes on the position of the π→π* band (see Table 1).

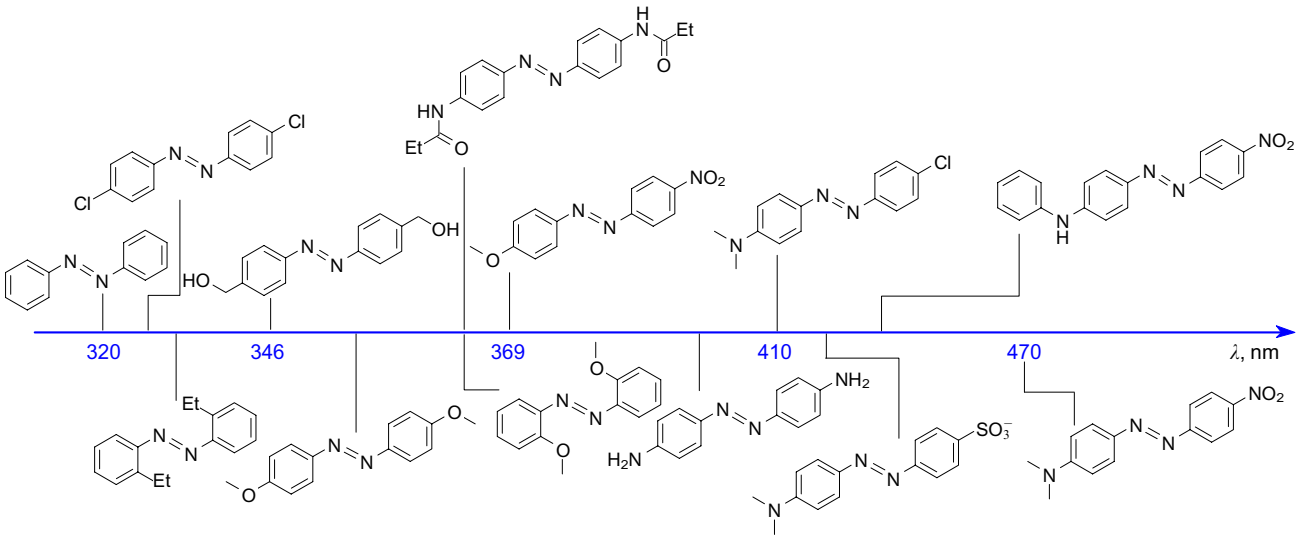


Figure 5. Effect of substituents in disubstituted azobenzenes on the position of the π → π* band in the absorption spectra (see Table 2).

Table 2. Positions of the π → π* transition bands in the absorption spectra and lifetimes for the *Z*-isomer of disubstituted azobenzenes $R^1C_6H_4N{=}NC_6H_4R^2$.

R^1	R^2	λ_{max}, nm	Solvent	$t_{1/2}$ (T, °C) [a]	Ref.
H	H	320 (443)	Ethanol	–	48
4-Cl	4-Cl	331	Cyclohexane	≈10.3 h (35)	58
2-Et	2-Et	334	Toluene	≈1.4 days (25)	59
4-CH_2OH	4-CH_2OH	346	Dichloro-methane	≈0.5 h (25)	63
4-OMe	4-OMe	358	Toluene	≈9.5 h (25)	59
4-NHC(O)Et	4-NHC(O)Et	364	–	≈5.2 h (25)	62
2-OMe	2-OMe	364	n-Heptane	≈7 days (25)	59
4-OMe	4-NO_2	369	Cyclohexane	≈51 μs (25)	66
4-NH_2	4-NH_2	394	–	≈4.7 min (25)	62
4-NMe_2	4-Cl	410	Cyclohexane	≈4.3 h (25)	58
4-NMe_2	4-SO_3^-	420	Acetone	≈1 h (25)	59
4-NHPh	4-NO_2	436	Cyclohexane	≈1.7 ms (25)	66
4-NMe_2	4-NO_2	470	See [b]	–	65

[a] Lifetime (half-life period) of the unstable *Z*-isomer; [b] a mixture of methylcyclohexane and methylcyclopentane.

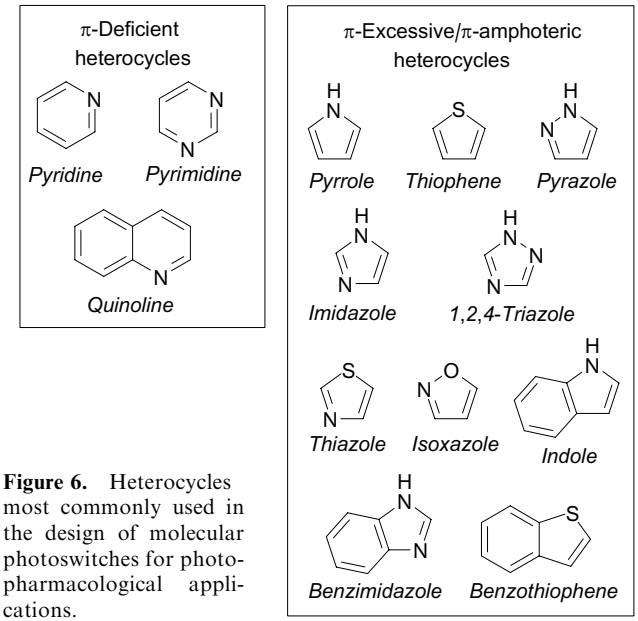


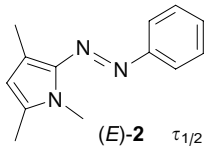
Figure 6. Heterocycles most commonly used in the design of molecular photoswitches for photopharmacological applications.

5.1.2. Azoheteroarenes

The replacement of the benzene ring of azobenzene with heteroaromatic rings offers new opportunities for the design of molecular photoswitches. The π → π* bands in the electronic absorption spectra of the *E*- and *Z*-isomers of azoheteroarene-containing π-excessive or π-amphoteric heterocycles are red-shifted as compared to similar bands of azobenzene. The replacement of the benzene ring with π-deficient aromatic heterocycles results in blue shift of these bands. Figure 6 shows heterocycles [40] that are most frequently used for the design of photopharmacological drugs. Currently, a large number of azoheteroarene-based switches with variation of both the heterocycles and substituents have been proposed.[68 – 74] In this Section, we address a molecular photoswitch the spectra of which exhibit the most pronounced red shift of the π → π* band relative to the analogous azobenzene band. Crespi *et al.* [40] proposed a more detailed review of other azoheteroarene derivatives.

Weston *et al.*[75] studied the photochemical properties of an azopyrrole photoswitch, namely, 1,3,5-trimethyl-2-(phenyldiazenyl)-1*H*-pyrrole (**2**). According to the π-excessive

Structure 2



(*E*)-**2** $\tau_{1/2}$ = 21 s (see [75])

Izomer	$\lambda_{max}(\pi\pi^*)$, nm	ε, L mol^{-1} cm^{-1}	$\lambda_{max}(n\pi^*)$, nm	ε, L mol^{-1} cm^{-1}
(*E*)-**2**	394	28 200	430	–
(*Z*)-**2**	346	7000	479	6000

character of pyrroles, the π → π bands of the *E*- and *Z*-forms in the spectrum of this compound in acetonitrile are red-shifted compared to those for azobenzene.

However, because of the significant overlap of these bands and their overlap with the n → π* bands, only partial photoseparation of the *E*- and *Z*-forms was achieved: the conversion rate (the content of the resulting *Z*-isomer, $\Gamma_{E\rightarrow Z}$) was 85 ± 3% when the compound was irradiated at 415 nm.

5.1.3. Protonation of the azo group nitrogen atoms. Azonium cations

As noted above, azobenzene is a very weak base,[54] however, the substitution of aromatic rings can seriously alter the acid – base properties of compounds.

The absorption spectrum of the azonium cation was obtained in aqueous ethanol with a high content of sulfuric acid,[54,56] and also in the gas phase.[76,77] The spectrum consists of three electronic vibrational bands [$\lambda_{max}(S_0 \rightarrow S_1)$ = 435 nm,[76,77] $\lambda_{max}(S_0 \rightarrow S_2)$ = 405 nm,[76] $\lambda_{max}(S_0 \rightarrow S_3)$ = 390 nm[76]]; the first band, in contrast to the absorption bands of the unprotonated azobenzene, is highly intense. It was shown that the first electronic vibrational band of the azonium cation corresponds to the π → π* transition, the maximum of which is considerably red-shifted in comparison to the π → π* transition band of azobenzene. This shift becomes possible due to two factors:[76]

— the energy of the σ-orbital of azobenzene after protonation is significantly decreased and the π-orbital becomes the HOMO;

— the energy of the LUMO π-orbital decreases because of the delocalization of the positive charge over the conjugated π-system.

Two other groups of electronic vibrational transitions correspond to π → π* transitions with the charge transfer from HOMO-1 and HOMO-2, which are localized on one of the benzene rings, to LUMO (Fig. 7).[76] Therefore, protonation of the nitrogen atom of the azo group can be used to develop a molecular switch with red-shifted absorption spectrum. This will be accompasnied by weakening of the N=N bond and, consequently, decrease in the lifetime of the thermodynamically less stable form.

Samanta *et al.*[78] demonstrated that substitution of all four *ortho*-positions of amino-substituted azobenzene with methoxy groups provides a high concentration of the protonated form of the *E*-isomer of the azonium cation at physiological pH (pK_a^E = 7.2). The absorption maximum for the band of the protonated form of compound **3**, 1,2-bis(2,6-dimethoxy-4-piperidinophenyl)-1-diazenium cation (**3**·H$^+$), is red-shifted (λ_{max} = 560 nm). Meanwhile, the concentration of the protonated form for the *Z*-isomer at physiological pH is significantly lower (pK_a^Z = 5.7). Although the measured lifetime of the *Z*-form was 10 s (at pH 7.5), owing to high intensity of the absorption band (ε = 20 000 L mol^{-1} cm^{-1} at 600 nm, pH 7), it is posssible to reach the photostationary equilibrium upon red light irradiation (λ = 635 nm, 80 mW cm^{-2} power density) within ~1 s.

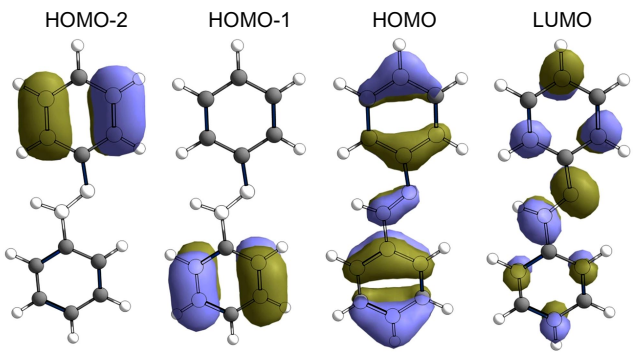
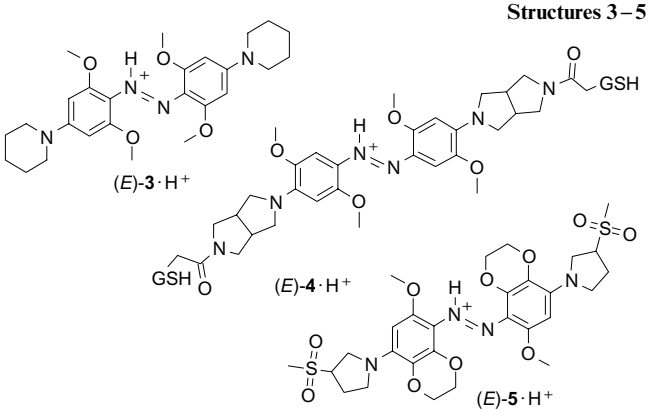


Figure 7. Molecular orbitals of the protonated form of azobenzene.

Dong *et al.*[41] studied a set of aminoazobenzene derivatives bearing methoxy groups in *meta*- and *ortho*-positions of the benzene ring. The main purpose of this study was to examine the possibility of attaining the largest red shift of the absorption bands. First, the authors relied on the empirical rule that the introduction of a methoxy group into the *meta*-position should result in a red shift of the absorption bands. The fact of this shift was confirmed by quantum chemical calculation using the TD-B3LYP/6-31++G**//B3LYP/6-31++G** method. Among four synthesized compounds, the maximum red shift (λ_{max} = 670 nm) was found for the protonated form of compound **4** bearing terminal glutathione moieties (γ-glutamyl-cysteinyl-glycine tripeptide). However, the use of such a switch at physiological pH is hindered due to the low pK_a value (5.4) of the *E*-isomer of the azonium cation **4**·H$^+$. Moreover, a sharp decrease in the *Z*-isomer lifetime (< 1 μs) was observed, making it impossible to reach the *Z*-state without the use of very intense light.

In a recent study, the same research group[79] suggested combining both approaches described above and substituting all *ortho*- and *meta*-positions of the benzene rings with methoxy groups. Since the preliminary computational modelling demonstrated that steric interaction between the adjacent methoxy groups in *ortho*- and *meta*-positions of one ring results in loss of the conjugation between the lone pair of oxygen atoms of the methoxy groups and the main π-system of the switch, the authors prepared an azobenzene derivative in which adjacent oxygen atoms in *ortho*- and *meta*-positions of the benzene ring formed a dioxane ring. The preliminary calculations (TD-B3LYP/6-31+G**//B3LYP/6-31+G method) indicated the presence of the necessary red shift in the absorption spectrum. For the further tuning of this spectrum and changing the pK_a value, the possibility to introduce various amino groups into the *para*-position of the benzene rings was considered. Below we present the structure and main characteristics of one of the newly synthesized compounds, namely, azobenzene **5**. The authors not only succeeded in attaining an intermediate shift of the absorption band of the azonium cation to longer wavelengths (λ_{max} = 597 nm) in comparison to the spectra reported in two preceding studies,[41,78] but also obtained the value of pK_a = 6.7, which means that 25% of molecules at physiological pH = 7.2 are in the protonated state. Due to high molar absorption coefficient of the azonium cation of this compound (138 000 L mol^{-1} cm^{-1} at 600 nm), the photostationary equilibrium can be attained within 0.1 s upon exposure to LED irradiation with a maximum emission at 720 nm (power density of 17 mW cm^{-2}). The period of thermal relaxation for the compound was measured to be 0.7 ± 0.1 s.

Structures 3 – 5



Compound	λ^{E}_{max}, nm	$\tau_{1/2}$, s	pK_a	Ref.
3·H$^+$	≈560	10 (pH 7.5)	7.2 (*E*), 5.7 (*Z*)	78
4·H$^+$	670	< 0.001	5.4 (*E*)	41
4	517	–	–	41
5·H$^+$	597	0.7	6.7 (*E*)	79

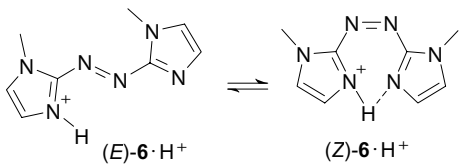
5.1.4. Protonation of other heteroatoms

Protonation of heteroatoms other than the azo group nitrogen atoms can also seriously alter the photochemical properties of a molecular photoswitch. In some cases, its characteristics can deteriorate, which must be taken into account when designing photopharmacological drugs.

Weston *et al.*[80] proposed a photoswitch based on imidazole core — (*E*)-1,2-bis(1-methyl-1*H*-imidazol-2-yl)diazene (**6**) (Scheme 2). The preliminary design of this switch was performed based on computational modelling of the structure and absorption spectra using the density functional theory method [CAM-B3LYP/6-311G(2df,2p)//B3LYP/6-31G(d,p)]. It was shown that for unprotonated *E*- and *Z*-forms of azoimidazole **6**, a good separation of the π → π* bands and a noticeable red shift of the absorption band compared to azobenzene spectrum should be observed. Such a molecular switch was synthesized and its photochemical characteristics were studied. It turned out that at pH 9, the spectral bands of neutral *E*- and *Z*-isomers, corresponding to π → π* transitions, were well-resolved in the positions of the maxima, differed in intensity, and red-shifted in comparison to the azobenzene spectrum, as was predicted by the computational modelling (λ^{E}_{max} = 405 nm, λ^{Z}_{max} = 350 nm). The lifetime of the neutral *Z*-form was 16 s. These parameters provided the stable photostationary state at pH 9 for this compound with the significant predominance of the metastable *Z*-form: $\Gamma_{E\to Z}$ (408 nm) = 90 ± 3%. Moreover, a reverse photoswitching effect at a different wavelength was found. The n → π* transition of the neutral *Z*-isomer of compound **6** (λ^{Z}_{max} = 495 nm, ε = 8000 L mol^{-1} cm^{-1} at pH 9) was much more intense than the similar transition of (*Z*)-azobenzene (see Fig. 2), thereby providing more efficient reverse transformation of the *Z*-isomer into the *E*-form than that in azobenzene (**1**).

However, all effects described above disappear at physiological pH. The absorption bands for the protonated *Z*- and *E*-forms of azoimidazole, 1-methyl-2-[(1-methyl-1*H*-imidazol-2-yl)diazenyl]-1*H*-imidazolium cation (**6**·H$^+$), significantly overlap, making the *Z* → *E*-photoswitching impossible. It should be noted that in contrast to protonation on the azo group nitrogen atom, the lifetime of this protonated *Z*-form of compound **6** increases to 352 s as compared to the unprotonated form. The pK_a values of *E*- and *Z*-forms were determined by photometric titration. Relying on these data, it can be concluded that photoswitch **6** can find application as a photomodulated acid or base. However, this is not enough for photopharmacological applications since protonation of the the heteroatom results in the loss of the photoswitching function at physiological pH.

Scheme 2



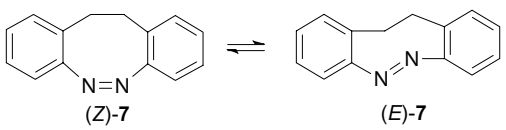
$\mathbf{t}_{1/2}$ = 16 s (for **6**), 352 s (for **6**·H$^+$)[80]

Isomer	pK_a	λ_{max}(ππ*), nm (at pH 9)	λ_{max}(nπ*), nm (at pH 9)	Ref.
(*E*)-**6**·H$^+$	4.7	394	430	80
(*Z*)-**6**·H$^+$	6.0	346	479	80

5.1.5. Steric effect of substituents in isomers. Bridged azobenzenes (dihydrobenzodiazocines)

The use of bridged derivatives of azobenzene, namely, dihydrobenzodiazocines **7** – **10**, due to the significant deformation of the planar geometry of the molecule, makes it possible not only to shift the n → π* absorption of both *E*- and *Z*-isomers to longer wavelengths and to increase the absorption intensity, but also to attain a significant resolution of these bands in absorption spectra.[81,82] Besides, a unique feature of this type of switches is that the *Z*-isomer is more thermodynamically stable than the *E*-form. Siewertsen *et al.*[81] showed that for dihydrobenzodiazocine **7** in n-hexane, λ_{max}(nπ*) is 404 and 490 nm for the *Z*- and *E*-isomers, respectively (Scheme 3). The *Z* → *E*-conversion was accomplished using a light-emitting diode with λ_{ex} = 385 nm and power (*W*) of 400 mW, with $\Gamma_{Z\to E}$ being ≈ 92%. The reverse switching from *E*- to *Z*-form can be driven either by photostimulation with a light-emitting diode at λ_{ex} = 520 nm ($\Gamma_{E\to Z}$ ≈ 100%) or under thermal conditions. In the latter case, $\tau_{1/2}$ = 4.5 ± 0.1 h at 28.5 °C. When hetero analogues **8** – **10** were used, the absorption maximum for the *E*-isomer was shifted to 559 nm.[83,84] Below are the photochemical characteristics of the mentioned compounds (ΔE_{rel} is the energy difference between *Z*- and *E*-isomers).

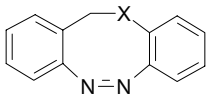
Scheme 3



$\tau_{1/2}$ = 4.5 h (28.5 °C)[81]

Isomer	λ_{max} (nπ*), nm	Γ (%) (conversion of isomers)	λ_{ex}, nm	Ref.
(*Z*)-**7**	404	92 (*Z* → *E*)	385	81
(*E*)-**7**	490	99 (*E* → *Z*)	520	81

Structures 8 – 10



8 – 10

Parameter	**8** (X = O) [83]	**9** (X = S) [83]	**10** (X = NH) [84]
ΔE_{rel}, kcal mol^{-1}	12.5	6.2	19.2
$\tau_{1/2}$ (T, °C)	89 s (20)	3.5 days (27)	131 s (25)
λ^{Z}_{max} (nπ*), nm	385	405	409
$\Gamma_{Z\to E}$ (%) (λ_{ex}, nm)	80 (385)	70 (405)	50 (405)
λ^{E}_{max} (nπ*), nm	525	525	559
$\Gamma_{E\to Z}$ (%) (λ_{ex}, nm)	99 (520)	99 (520)	> 99 (520 – 690)

5.1.6. Electronic effect of substituents in isomers

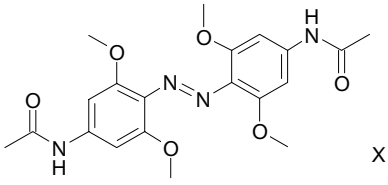
Beharry *et al.*[44] studied the influence of *ortho*-methoxy groups in benzene rings on the spectral properties of 4,4′-diacetamidoazobenzene in dimethyl sulfoxide. Although the π → π* band in the spectrum of (*E*)-2,2′-dimethoxy-4-4′-diacetamidoazobenzene demonstrated the expected red shift, in the case of 4,4′-diacetamido-2,2′,6,6′-tetramethoxyazobenzene (**11**), the π → π* band was blue-shifted and had moderate intensity (λ_{max} = 338 nm, ε_E = 16 170 L mol^{-1} cm^{-1}) in comparison to the spectrum of unsubstituted 4,4′-diacetamidoazobenzene. Here, for the n → π* band, a significant red shift and increased intensity (λ_{max} = 480 nm, ε_E = 4030 L mol^{-1} cm^{-1}) were observed. A study of the optical properties of compound **11** revealed that in the spectrum of *Z*-isomer, the n → π* band is blue-shifted by 36 nm compared to that for the *E*-isomer.

A similar, albeit much less pronounced effect was also observed by other researchers. Thus, studies[85,86] were focused on the spectral properties of azobenzenes bearing four *ortho*-alkyl substituents. The resolution of n → π* absorbances of the *E*- and *Z*-isomers allowed for the use of 4,4′-diacetamido-2,2′,6,6′-tetramethoxyazobenzene (**11**) as a molecular switch that was photoactivated in both directions; the following values were obtained: $\Gamma_{E\to Z}$ = 80% (530 – 560 nm) and $\Gamma_{Z\to E}$ = 85% (450 – 460 nm). Assuming that compound **11** could find photopharmacological application, the authors also studied its spectral and photochemical properties in a phosphate buffer solution (25 mM, pH 7). It was shown that the desired properties were preserved and the switch could be used in aqueous solutions at physiological pH: $\Gamma_{E\to Z}$ = 70% (530 – 560 nm), $\Gamma_{Z\to E}$ = 80% (450 – 460 nm) at 25 °C.

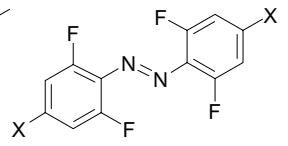
The lifetime of the *Z*-form of switch **11** in an aqueous solution ($\tau_{1/2}$ = 53 h) was measured and its acid – base properties were studied (pK_a = 3.8). Beharry *et al.*[44] demonstrated the insufficient stability of this compound under glutathione reduction conditions, which may impede its *in vivo* application. To explain the shift of the n → π* band, a computational modelling (the TD-B3LYP/6-31G*//B3LYP/6-31G* method) of the electronic spectra of compound **11** and its analogue containing no *ortho*-methyl groups was carried out. A considerable shift of the n → π* band in the spectrum of (*E*)-4,4′-diacetamido-2,2′,6,6′-tetramethoxyazobenzene (**11**) in comparison to the spectrum of (*E*)-4-4′-diacetamidoazobenzene and the virtual absence of the difference between the spectra of the same compounds existing in *Z*-forms can be attributed to stronger interaction between the σ-orbital located on the azo group (HOMO) and lone pair orbitals of the oxygen atom of the methoxy group in the *E*-isomer as compared to the *Z*-form.

A similar strategy of changing the σ-orbital energy *via* introducing a σ-electron-withdrawing group into the *ortho*-position was used when designing photoswitches based on tetra-*ortho*-halo-substituted azobenzenes.[87,88] Bléger *et al.*[87] studied spectral and photochemical properties of 2,2′,6,6′-tetrafluorobenzene (**12**). The spectrum of the *E*-form of tetrafluoro-substituted azobenzene in acetonitrile and other solvents differs insignificantly from that of the *E*-form of azobenzene [λ_{max} (ππ*) = 305 nm, λ_{max} (nπ*) = 458 nm]. However, for the n → π* absorption band of the *E*-form, a 42 nm blue shift was found. Thus, an effective forward and reverse photoswitching of this compound with $\Gamma_{E\to Z}$ = 91% (450 nm) and $\Gamma_{Z\to E}$ = 86% (410 nm) was implemented. The thermal stability of the *Z*-form of switch **12** proved to be very high, $\tau_{1/2}$ = 700 days at T = 25 °C, and ΔE_{rel} was 28 kcal mol^{-1}. Below are photochemical characteristics of azobenzenes **11** and **12** and also of a *para*-ethoxycarbonyl-substituted analogue, compound **13**.

Sructures 11 – 13



11



X = H (**12**), CO_2Et (**13**)

Parameter	**11** (see [44])	**12** (see [87])	**13** (see [87])
$\tau_{1/2}$ (25 °C)	53 h (buffer)	700 days	–
λ^{Z}_{max}, nm	444 (nπ*)	~280 (ππ*),	~260 (ππ*),
		416 (nπ*)	419 (nπ*)
$\Gamma_{Z\to E}$ (%) (λ_{ex}, nm)	85 (450 – 460)	86 (410)	97 (410)
λ^{E}_{max} (nm)	338 (ππ*),	305 (ππ*),	314 (ππ*),
	480 (nπ*)	458 (nπ*)	469 (nπ*)
$\Gamma_{E\to Z}$ (%) (λ_{ex}, nm)	80 (530 – 560)	84 (313)	90 (> 500)
		91 (450)	

Thus, strategies have now been developed for shifting the absorption maximum of photoswitches to the visible region up to 670 nm. To obtain compounds with absorption bands shifted to the infrared region, further research is needed. A promising approach is the use of two-photon spectroscopy to study the isomerization processes.

5.2. Optimization of properties required for the stability of a photopharmacological drug *in vivo*

An important issue that is worth noting when developing azobenzene photoswitches for *in vivo* applications is stability of the compounds against reduction in the body. Indeed, the intracellular medium contains glutathione in concentrations of up to ≈10 mmol L^{-1},[89] and its ability to reduce azobenzenes to 1,2-diarylhydrazine derivatives should be considered in the design of an azobenzene-based photopharmacological drug.[78,79,89–91] It was demonstrated that the reduction mechanism includes the step of an attack by a glutathione sulfur atom on the azo group to generate a sulfenylhydrazide intermediate and the subsequent addition of a second glutathione molecule to give a 1,2-diarylhydrazine derivative and oxidized glutathione.[89,90] In this case,

the sulfenylhydrazide intermediate can hydrolyze back to the azo compound in the deficiency of glutathione.

It was established that the rate of reduction of azobenzene derivatives with glutathione can be decreased by introducing electron-donating substituents into all *ortho*-positions of benzene rings. These substituents can be exemplified by thiol [91] and methoxy groups,[41] and also chlorine [78] and fluorine atoms.[92] Stability to the reduction with glutathione also increases upon the introduction of bulky amino groups into *ortho*-positions of the photoswitch.[93] Another strategy applied to improve the electron enrichment of azo compounds includes the use of their heterocyclic analogues. This approach was implemented by Stricker *et al.*,[94] who proposed to use heterocyclic arylpyrazoles, which are stable to reduction with glutathione.

Enzymatic reduction representing another type of reactions involving azobenzene cores within the cells has been studied much less extensively. In living organisms, azo dyes are reduced by the azoreductase – nicotinamide adenine dinucleotide phosphate (NADH) system.[95] Living microorganisms that form the endogeneous intestinal microflora (microbiome) also reduce azo compounds, which is crucial for the metabolism of drugs meant for oral administration.[96] The photoswitch stability towards such reduction systems is unexplored at the moment, although the processes involving them have long been known in pharmacology. For example, one of the earliest antimicrobial drugs prontosil is a prodrug, and its active sulfanylamide form is generated *via* the reduction of the N=N bond.[97]

6. Key methods for the computational modelling used for the molecular design of photopharmacological drugs

6.1. Modelling of the spectral properties of azobenzenes

According to the results of the quantum chemical studies, experimental λ_{max} values for the first and second absorption bands for *Z*- and *E*-azobenzenes can be reproduced with the use of relatively inexpensive computational approaches based on the density functional theory (DFT). Various functionals have been tested, the most accurate result being obtained with the use of the TD-CAM-B3LYP//B3LYP approach (the molecular geometry was optimized using the B3LYP functional, the spectrum was calculated with the TD-CAM-B3LYP method).[98] The use of computationally more demanding *ab initio* methods (RASPT2, EOM-CCSD) provided better correlation with the experimental data,[98] however, the difference in accuracy was insignificant in terms of the computational screening. In the case of the azonium cation, the $S_0 \rightarrow S_1$ transition also demonstrated a satisfactory correlation between the values of the absorption maxima calculated using various methods: λ_{max} = 382 [TD-CAM-B3LYP/def2-TZVP//ωB97X-D/6-311+G(2df,p)] and 406 nm [EOM-CC2/def2-TZVP//ωB97X-D/6-311+G(2df,p)], with the experimental value being λ_{max} = 435 nm.[77]

Calculations have been performed for a variety of substituted azobenzenes to determine a method capable of reproducing the experimental absorption maxima.[83, 99 – 103] It was demonstrated that to calculate the absorption spectrum of unprotonated and singly protonated derivatives of azobenzene, the optimal balance between the accuracy and the computational cost is achieved by using TD-CAM-B3LYP//B3LYP and PBE0//PBE0 density functional theory approaches. The minimum basis set that can be employed is 6-31G* or its analogues. When optimizing the geometry of compounds with strong steric interactions of substituents, one should consider dispersion corrections to the density functional [104] and make use of B3LYP-D and PBE0-D functional forms. It can be expected that Minnesota density functionals (M1 and other) will also provide good results for geometry optimization and simulation of the spectra, but to get statistically valid data, further research is needed.

The question also remains of the quality of the results obtained with the density functional theory methods for azobenzenes protonated at both nitrogen atoms of the double bond. However, not a single photoswitch has been proposed in which both nitrogen atoms of the azo group would be protonated at physiological pH; therefore, this issue is rather of theoretical than of practical interest. Double protonation of the azo group nitrogens strongly compromises the integrity of the π-system, and the error of CAM-B3LYP method, which was originally developed to describe the charge transfer processes in large π-systems, is expected to increase.

To be successfully implemented, *in silico* screening of the absorption maxima of azobenzene derivatives should start from the calculation of the pK_a values of the acid – base groups of the potential drug with the subsequent calculation of λ_{max} carried out least at the TD-CAM-B3LYP/6-31G*//D-B3LYP/6-31G* level of theory. However, for photopharmacological molecules, which can consist of hundreds of atoms, this approach can be computationally expensive. Further progress in this field can be made if less costly methods for calculating the absorption maximum, which nevertheless retain an acceptable accuracy, are proposed. Attempts to use semiempirical methods based on molecular orbital theory (*e.g.*, AM1) failed.[101]

Calbo *et al.*[105] used a test set consisting of dozens of various azoheteroarenes to study the correlations between the absorption maxima calculated at the TD-PBE0/6-31G**//PBE0/6-31G** level of theory, and orbital energy differences corresponding to the transition under consideration, which were calculated with PBE0/6-31G**//PBE0/6-31G. For the *E*-form, correlations were found for both the $\pi \rightarrow \pi^*$ transition (coefficient of determination $R^2 = 0.7841$) and for the $\sigma \rightarrow \pi^*$ transition ($R^2 = 0.8188$). However, for the *Z*-form such correlation was retained solely for the $\pi \rightarrow \pi^*$ transition ($R^2 = 0.9184$), but was not observed for the $\sigma \rightarrow \pi^*$ transition ($R^2 = 0.3386$). Since a correlation ($R^2 = 0.5373$) between the N=N bond order characterized by the Wiberg indices [106] and the *Z*-isomer lifetime has been established, the main characteristics of the photoswitches of this type could be assessed with computational costs determined by the geometry optimization using the density functional theory.[105] However, these approaches should be applied with particular caution.

As for the entire computational chemistry, approaches based on machine learning seem to be the most promising. Recently, Thawani *et al.*[107] demonstrated that an empirical model, the parameters of which were determined using machine learning algorithms, allowed for calculation of the absorption maxima for a test set of azobenzenes with an error comparable to that of the time-dependent density functional theory (TD-DFT).

6.2. Modelling of relative energies of isomers and thermal isomerization of azobenzene derivatives

Various methods were employed to calculate the relative Gibbs energies of the *E*- and *Z*-isomers of azobenzene and its azonium cation, ranging from the density functional theory and Möller – Plesset perturbation theory (MP2) to coupled cluster (CC) method and complete active space 2nd order perturbation theory (CASPT2).[53, 76, 77, 108 – 112] The calculation results are presented in Table 3. The results revealed that the ground states of azobenzene derivatives are well defined by a single-configuration wave function, and there is no necessity to use multiconfiguration approaches, as the difference between the values obtained by the CASPT2 and MP2 methods is negligible and can be attributed to the application of different methods of geometry optimization. Dynamic correlation is of high importance; however, as can be seen from Table 3, it is well reproduced by the DFT B3LYP-3D method: the values calculated by this method are very close to those obtained by MP2 calculations and deviate by less than 1 kcal mol^{-1} from those calculated by the coupled cluster singles and doubles (triples) excitations [CCSD(T)]. It is noteworthy that the dispersion corrections should be taken into account, since otherwise, the B3LYP method provides much more significant deviation than the MP2 and CCSD(T) approaches.

Based on analysis of the reported data for a variety of azobenzene derivatives, the following may be stated. The optimal techniques suitable for the calculation of energy values to within several kcal mol^{-1} are the density functional theory methods using the B3LYP and PBE0 functionals and applying the dispersion corrections[104] (B3LYP-D and PBE0-D) or Minnesota functionals (M11, M06). The entropy contributions can be found by calculating the partition function based on vibrational frequencies, which are calculated by the same methods. To take into account the solvent (water), the polarizable continuum model (PCM) can be used.

Modelling of the transition states for the thermal isomerization of molecular switches is not such an easy task for computational chemistry as modelling of the ground states. As mentioned above, thermal isomerization of azobenzenes can occur by two competing mechanisms, namely, rotational and inversion ones. Despite the obvious multiconfiguration character of the diradical rotational transition state, in most publications, transition states were modelled with the use of single-configuration density functional theory methods (B3LYP, PBE-0). These results cannot be considered reliable due to poor treatment of the static electronic correlation. Attempts to optimize the rotational transition state using single-configuration methods often lead to the artifact geometry shifted towards the inversion transition state. On the other hand, although the inversion transition state is virtually single-configuration, it has a considerable charge transfer and, hence, requires special attention when considering dynamic electronic correlation.

Table 3. Relative Gibbs energies for *E*- and *Z*-isomers of azobenzene (ΔE_{rel}) and transition state energies for the inversion (TS Inv/Z) and rotational (TS rot/Z) pathways of the isomerization reaction calculated by various quantum chemical methods.

Method	ΔE_{rel}	Ref.	TS Inv/Z (TS rot/Z)	Ref.
CASPT2/6-31G*// CASSCF/6-31G*	11.9	53	(38.1)	53
CASSCF/6-31G*// CASSCF/6-31G*	16.4	53	(41.5)	53
MP2/6-31G*// B3LYP/6-31g*	12.27	108	53.03	108
MP2/6-31G*//MP2/6-31G*	12.9	109	47.8	108
B3LYP/6-31G*// B3LYP/6-31G*	15.2	108	40.52	108
B3LYPD3/6-31G*// B3LYPD3/6-31G*	12.7	109	40.0	109
CCSD/6-311++G**// CCSD/6-31G*	13.5	109	47.6	109
Experimental value	10 – 12	48	≈33 – 35	43, 48

Note. All values are given in kcal mol^{-1}.

As can be seen from the data in Table 3, it is impossible to reproduce the energy value of the inversion transition state for azobenzene obtained with MP2 and CCSD using the density functional theory B3LYP-3D method, as the deviation is 15%. Therefore, for a reliable calculation of comparative energies of two types of transition states, methods that take into account both dynamic and static electronic correlations (RASPT2, CASPT2, NEVPT, MRCI) should be preferred.† Unfortunately, the conclusions derived from modelling of the transition states of thermal isomerization with DFT methods should be interpreted with great caution. Mention should be made of the results of quantum chemical calculations suggesting that triplet states might be involved in the photoisomerization process; however, no direct experimental evidence of this hypothesis has yet been found.[53]

Another promising approach for fast screening of thermal lifetimes is to find the correlation between the N=N bond length in the ground state structure and thermal lifetime. However, for the development of such approach additional research is needed.

6.3. Methods for estimating the ligand – receptor binding affinity

The methods used in photopharmacology to estimate the binding affinity between a potential drug (ligand) and a receptor do not differ from those used in classical pharmacology. In this Section, a brief overview of these methods and examples of their application to address the photopharmacological problems is given.

Methods for the calculation of ligand – receptor binding free energy can be divided into three groups, differing significantly both in accuracy and computational costs.

1. Docking methods.

To calculate the receptor – ligand binding Gibbs free energy by docking methods, empirical functions of two types are applied. The first type includes empirical functions that simulate Gibbs energy, the second type includes functions which are derived from the structural databases of receptor – ligand complexes.[113, 114] Such computational approaches are effective and, despite their relatively low accuracy, they are employed in screening of a large number of potential ligands. In recent years, docking methods have been widely used in photopharmacology both for the interpretation of experimentally observed effects and for

† RASPT2 is the restricted active space second-order perturbation; NEVPT2 is the N-electron valence state second-order perturbation theory; MRCI is the multireference configuration interaction.

the *in silico* design of photoactivated drugs.[27, 28, 115 – 117] Pinto and Mascharak[27] used docking to explain the increased activity of one of the photoactivated ligands, namely, azoLPA, which is an azobenzene photoswitch that allows for the optical control of lysophosphatidic acid (LPA) receptor activation. The computational modelling made it possible to reveal the difference in the mechanisms and efficiency of binding of various derivatives of this ligand to receptors. Westphal *et al.*[115] utilized docking in design of a photoactivated Δ^9-tetrahydrocannabinol, a ligand for cannabinoid receptor CB1. A mechanism for the binding of such a ligand to the receptor was proposed, and its most effective analogues were found. Cabré *et al.*[116] used docking to identify the ligand (bridged azobenzene) that binds most efficiently to the kainate receptor GluK2. It was demonstrated that the mechanism of binding of the proposed bridged azobenzenes is similar to that for the known ligand GluAzo, which is an azobenzene – glutamate conjugate.

2. Methods that simulate the pathway between the two limiting states — a free receptor and a ligand and the receptor – ligand complex.

This pathway consists of a series of intermediate states and can be either physically realistic, that is representing a realistic way of the ligand – receptor binding or artificial ('alchemical').[118 – 120] To calculate the Gibbs free energy difference between the two limiting states, free energy perturbation or thermodynamic integration methods are used most often. These methods require the simulation of Boltzmann distribution of configurations in each of the final and intermediate states. To simulate configurations, methods of molecular dynamics, Monte Carlo[121] and their combinations are applied.[122] These methods demonstrate the highest accuracy but require large computational efforts.

3. Methods simulating only two limiting states of the system, that is, free receptor and ligand and the receptor – ligand complex.

Among such approaches, the most commonly used are hybrid methods, in which ligands are described by a molecular-mechanical force field, while the effect of surroundings is described by the continuum model, *e.g.*, generalized Born surface area model (MM/GBSA) or Poisson – Boltzmann surface area model (MM/PBSA).[123, 124] In these methods, the Gibbs free energy of the ligand – receptor binding includes three terms:

— the internal energy difference between two states of the system;

— the solvation Gibbs free energy difference, for the calculation of which the implicit solvent model is applied;

— the change in conformational entropy of the system, which is calculated by means of normal mode analysis.

The calculation of entropy contribution requires the largest computational effort, with the calculation accuracy being low and often giving only rough estimates.[124, 125] An alternative to MM/GBSA and MM/PBSA approaches is the linear interaction energy method, in which the mean energy difference of the ligand interaction with the surrounding is calculated for two states: a ligand bound to the receptor in a solvent and a free ligand in a solvent.[125] In all three methods, averaging is performed over an ensemble of configurations generated by molecular dynamics simulations, Monte Carlo simulations, or their combination.

The second and the third groups of methods are only beginning to be used in the development of photopharmacological drugs. Day *et al.*[126] employed the MM/GBSA methods to calculate the binding energies for photoactivated peptides functionalized with azobenzene derivatives to the VCAM1 receptor, a peptide belonging to the immunoglobulin superfamily. The calculations revealed peptides that effectively bound in the dark state ($\Delta G < -8$ kcal mol^{-1}) and were not bound in the photoactivated form ($\Delta G > 2$ kcal mol^{-1}). Based on the modelling, candidates for the further optimization of the structure and experimental validation were chosen. Despite the relatively low accuracy, docking is considered to be the most suitable for large-scale screening.

The advantages of the methods of the second and third groups become obvious only if a sufficiently accurate estimation of the Gibbs free energy of the binding process is possible. In turn, the accuracy of methods for calculating this energy is determined by a number of factors.[119, 127, 128]

The first factor is the accuracy of the parameters of the energy function (force field) used to calculate the molecular dynamics trajectories or perform Monte Carlo sampling. A series of available force fields for common amino acids, water, and physiologically relevant ions is known, allowing for the calculation of the energy difference to within a few kilocalories (AMBER,[129] CHARMM[130] and other). However, there are currently no common force fields for organic molecules, providing the same accuracy. To improve the accuracy, hybrid quantum mechanical/molecular mechanical (QM/MM) methods were applied is several studies. In this case, the biotarget cofactor and the ligand were calculated by quantum mechanical methods, and the protein surroundings, water molecules, and ions were calculated using the force fields.[131, 132] However, high computational costs hamper the widespread application of the QM/MM methods for drug design. On the other hand, machine learning techniques for the force field parameterization have been extensively developing in recent years.[133, 134] Their application to determine molecular mechanical force field parameters for the ligand and the receptor cofactor can significantly improve computational accuracy.

The second important factor is the accuracy of the starting structure of the biotarget – ligand complex used in modelling, including the correct states of protonation of the acid – base groups of the protein and the ligand, as well as the presence and position of water molecules at the binding site. The best choice is the structure of the complex obtained by X-ray crystallography. If the crystallographic structure is not available, homology modelling techniques can be used to predict the structure of the biotarget[135, 136] and docking techniques are applicable for an initial check of possible binding sites.[113, 114] However, such a strategy reduces the accuracy and increases the computation time.

However, neither crystallographic structure nor the structure obtained by homology modelling methods contain information on the state of protonation of acid – base groups. To calculate the pK_a values, various computational approaches are used which are considered in several reviews (see, *e.g.*, Refs 137, 138). Additional complexity is the possibility to alter the pK_a values of some acid – base groups during molecular dynamic modelling. In this case, molecular mechanical methods should be used which take into account the possibility of dissociation or addition of protons in the process of modelling, for example, the pH-constant molecular dynamics method.[139, 140]

It is also worth emphasizing the special role of incorporation the water molecules in the modelling of biological

structures. For example, water molecules were shown to influence both the value of the Gibbs free energy of binding and the ligand configuration upon binding to the receptor.[141–143] Determination of number, localization, and structural organization of water molecules in the cavities of protein molecules is a challenge in view of the complexity of detecting water molecules by X-ray crystallography.[144, 145] Computational methods are also used to predict the presence and positions of water molecules,[146, 147] and the proper choice of the suitable technique is critically important for obtaining reliable computational models.[148]

7. Main approaches to the synthesis of azobenzene- and azoheteroarene-based molecular switches

7.1. Synthesis of azobenzene-based photoswitches

The most common strategies for the synthesis of azobenzene switches are illustrated in Scheme 4 and include the following processes:

— azo coupling reaction (path *a*),

— coupling of anilines with nitroso compounds (the Mills reaction) (path *b*),

— oxidative coupling of anilines (path *c*),

— reductive coupling of nitroarenes (path *d*),

— dehydration of 1,2-diarylhydrazines (path *e*),

— reduction of azoxybenzenes (path *f*),

— coupling of arenehydrazonium salts with aryllithium derivatives (path *g*),

— palladium-catalyzed coupling of arylhydrazines with aryl halides (path *h*),

— reaction of quinones with arylhydrazines (path *i*),

— Wallach reaction (path *j*),

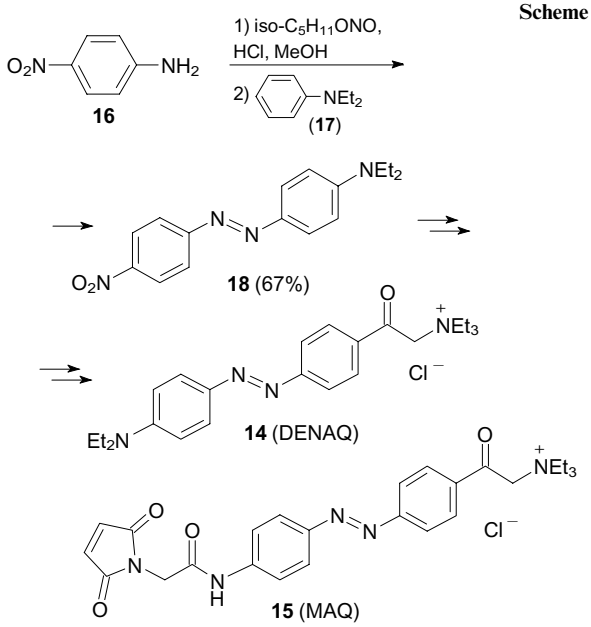
— reaction of triazenes with anilines or phenoxides (path *k*).

7.1.1. Azo coupling reaction

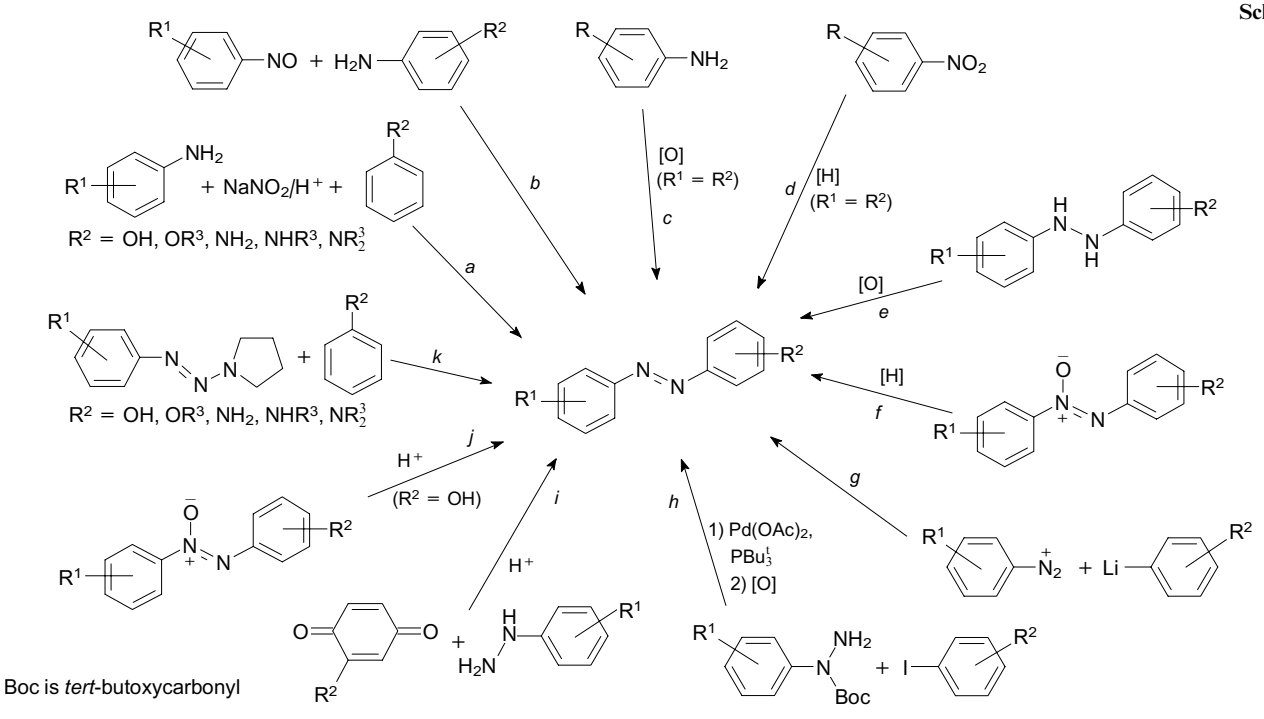
Azo coupling is the reaction between arenediazonium salts and aromatic amines and phenols. The main drawbacks of this approach include the instability of arenediazonium salts at room temperature, low yields, a limited set of the reactants in use, and pollution of the environment with acidic and alkaline wastewaters. This transformation is used to prepare a variety of azobenzene-containing drugs, *e.g.*, first- and second-generation photocontrolled potassium channel blockers such as quaternary ammonium salts based on diethylamino- (**14**, DENAQ)[149] and maleimido-substituted azobenzenes (**15**, MAQ)[150] (Scheme 5). The synthesis of photoswitch DENAQ (**14**) as illustrated in Scheme 5 starts from the azo coupling of 4-nitroaniline (**16**) with *N*,*N*-diethylamine (**17**), leading to asymmetric azobenzene derivative **18** in a moderate yield.

Since the azo coupling reaction is widely used in the industrial production of azobenzene dyes, environmentally friendly protocols of its implementation have been elaborated.

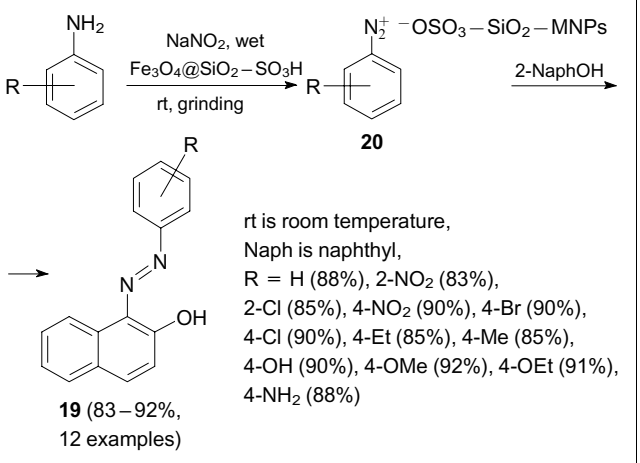
Scheme 5



Scheme 4



Scheme 6

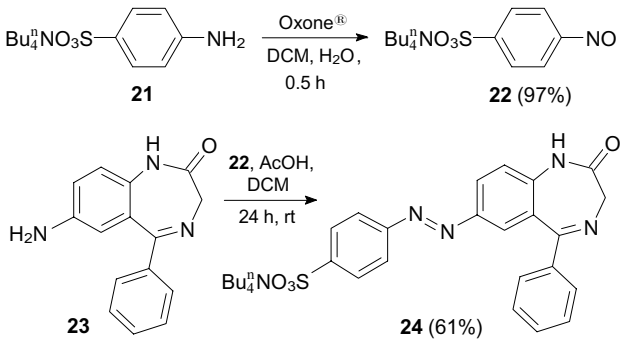


One of the strategies for the synthesis of arylazonaphthols **19** by this reaction implies the use of solid acids such as $Fe_3O_4@SiO_2-SO_3H$ magnetic nanoparticles (MNPs) (Scheme 6), thereby reducing the amount of acidic and alkaline wastewaters in the environment. Diazonium salts **20** react with 2-naphthols at room temperature in the absence of solvents.[151]

7.1.2. Mills reaction

The Mills reaction is the reaction between aromatic nitroso compounds and anilines in the presence of glacial acetic acid. An advantage of this method is a wide spectrum of reactants since many anilines can be oxidized to nitroso compounds. An approach has been elaborated, involving the use of Oxone ($2\,KHSO_5 \cdot KHSO_4 \cdot K_2SO_4$, Oxone®) or potassium peroxomonosulfate in a water/dichloromethane two-phase system.[152] With the use of this method, aniline **21** was converted into 4-nitrosobenzenesulfonate **22**, which was then reacted with 7-amino-5-phenyl-1,3-dihydro-2*H*-benzo[*e*][1,4]diazepin-2-one (**23**) (Scheme 7).[153] The product **24** (Azo-NZ1) exists mainly in the *E*-configuration and blocks γ-aminobutyric acid (GABA) receptors.

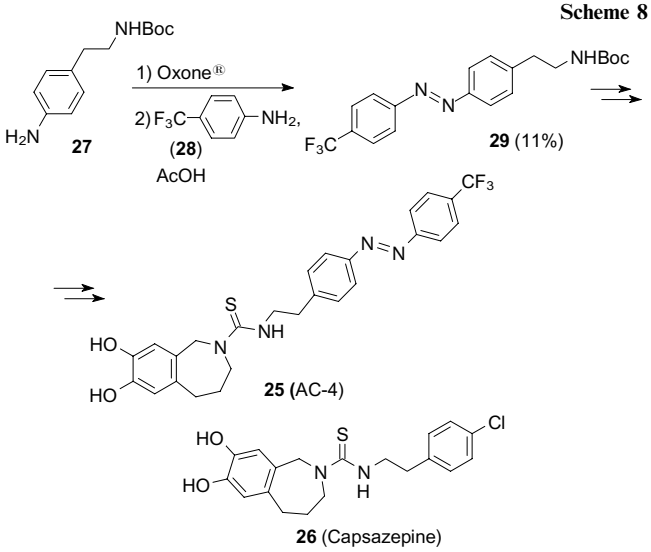
Scheme 7



Another example of the synthesis of photopharmacological drug *via* the Mills reaction using Oxone as an oxidant is the preparation of compound **25** (AC-4), an analogue of the photoswitchable drug Capsazepine (**26**), which is a TRPV1-receptor antagonist‡ (Scheme 8).[154]

‡ TRPV1- is the transient receptor potential cation channel subfamily V member 1.

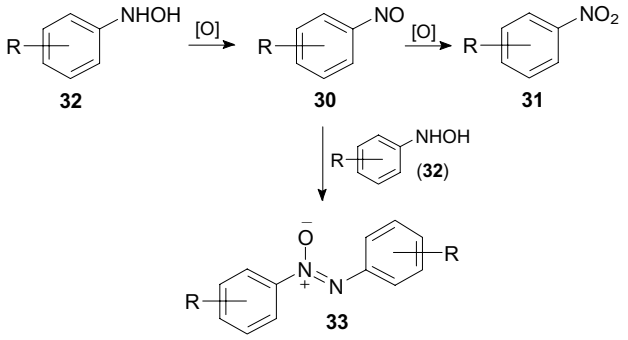
Scheme 8



Protected 4-(2-aminoethyl)aniline **27** was first oxidized to an intermediate nitroso compound, and then condensed with 4-trifluoromethylaniline (**28**) to give azobenzene derivative **29**, which subsequently provided product **25**.

Nitroso compounds can be synthesized by oxidation of arylhydroxylamines. Various reagents are used as oxidants, *e.g.*, $KMnO_4$,[155] $K_2Cr_2O_7-H_2SO_4$ system,[156] *m*-chloroperoxobenzoic acid (*m*-CPBA),[157] pyridinium chlorochromate (PCC),[158] K_2FeO_4 (see Ref. 159), *etc.*[160] However, nitrosoarenes **30** are often oxidized further to nitroarenes **31**, which is a significant drawback of this approach. Moreover, when the starting compound is *N*-arylhydroxylamine **32**, it can condense with nitroso compounds **30** to afford azoxybenzenes **33** (Scheme 9).[160]

Scheme 9

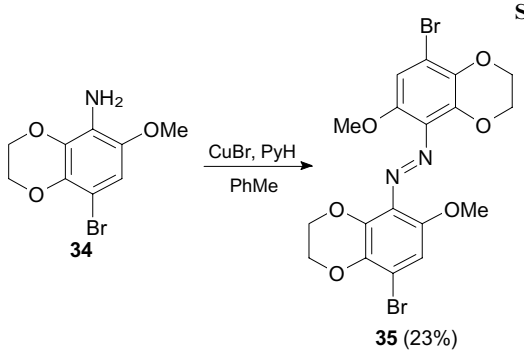


7.1.3. Oxidative coupling of anilines

Oxidative coupling of amines enables the synthesis of exclusively symmetrical azobenzenes. Anilines (*e.g.*, **34**) react with copper(I) bromide in the presence of pyridine (PyH) to give azobenzene derivatives in good yields. This approach was utilized by Dong *et al.*[79] to prepare photoswitch **35** showing absorbance in the near-IR region (Scheme 10).

The oxidands used in this reaction may be represented by a variety of compounds such as silver salts, oxides, and complexes,[161 – 163] lead tetraacetate,[164] hypervalent iodine compounds,[165] horseradish peroxidase – H_2O_2 system.[166] *etc.* Presently, MnO_2, $KMnO_4$, such systems as $HgO-I_2$ (Ref. 167) and $KMnO_4-CuSO_4 \cdot 5\,H_2O$ (Ref. 78), and a

Scheme 10



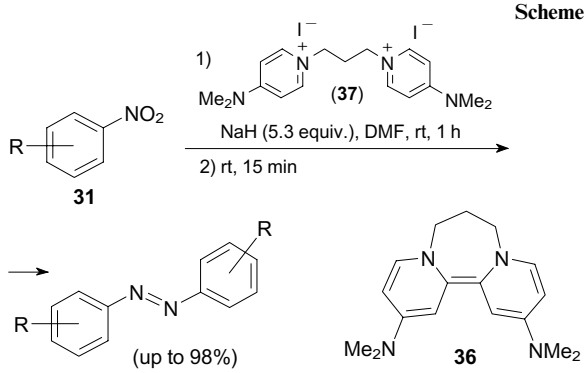
mixture of *N*-chlorosuccinimide (NCS) with diazabicyclo[5.4.0]undec-7-ene (DBU) are most frequently used.[168]

7.1.4. Reductive coupling of nitroarenes

Reductive coupling of aromatic nitro derivatives also provides exclusively symmetrical azo compounds. As reducing agents, complex hydrides,[169, 170] zinc,[171] or glucose [172] in a basic medium are mainly used.

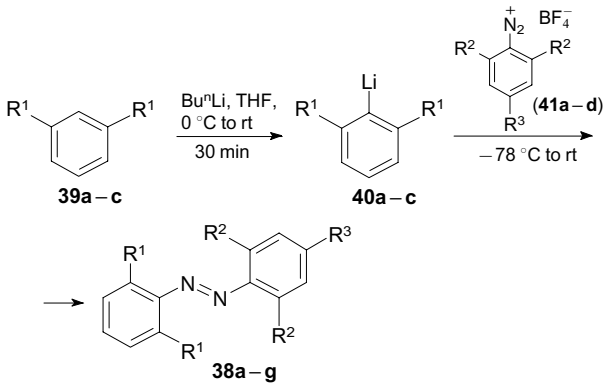
Recently, Nozawa-Kumada [173] proposed a method for producing azobenzenes and phenazines *via* coupling of nitrobenzenes **31** in the presence of organic super-electron-donating molecules. The reaction proceeds under mild conditions, requires no metal catalysis, and is suitable for a wide variety of nitroarenes (Scheme 11). The active form of an organic catalyst (structure **36**) is generated under mild conditions from the corresponding pyridinium salt **37**.

Scheme 11



R = H (98%), 4-Me (70%), 3-Me (98%), 2-Me (38%), 4-Bu^t (95%), 4-OMe (79%), 4-F (51%), 3-F (65%), 4-Cl (80%), 3-Cl (71%), 2-Cl (74%), 4-Br (68%), 3-Br (71%), 4-CN (72%), 4-CO_2Bu^t (57%)

Scheme 12



38: R^1 = R^2 = OMe: R^3 = H (**a**, 86%), OMe (**b**, 81%); R^2 = OMe, R^3 = H: R^1 = F (**c**, 82%), Cl (**d**, 86%); R^3 = H: R^1 = R^2 = F (**e**, 77%), Cl (**f**, 92%); R^1 = Cl, R^2 = F (**g**, 77%);
39, **40**: R^1 = OMe (**a**, > 98%), F (**b**, 31%), Cl (**c**, 46%);
41: R^2 = OMe: R^3 = H (**a**, 86%), OMe (**b**, 81%);
R^3 = H: R^2 = F (**c**, 77%), Cl (**d**, 92%)

7.1.5. Coupling of arenediazonium salts with aryllithium derivatives

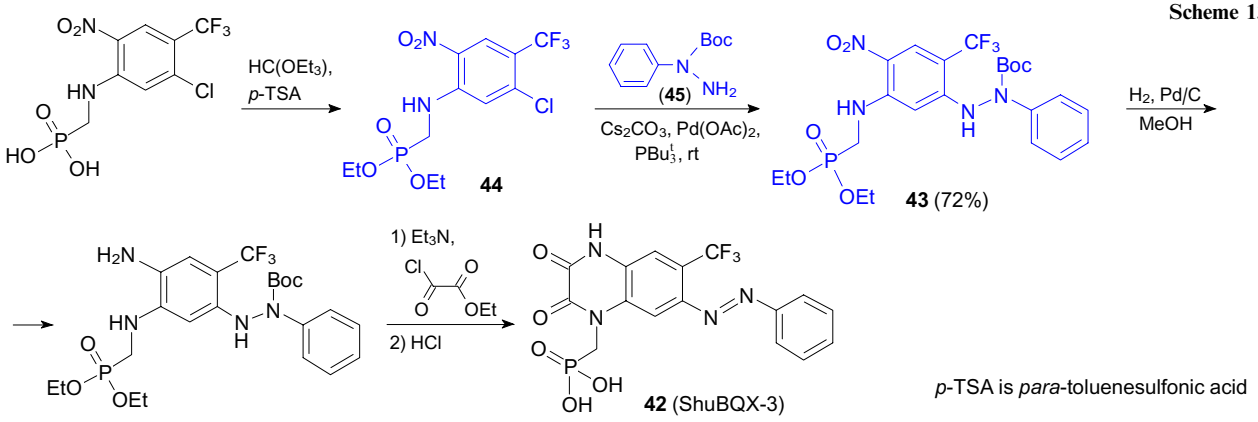
A strategy based on the coupling of arenediazonium salts with aryllithium derivatives is suitable for the synthesis of unsymmetrical azobenzene derivatives. It includes the preparation of an arenediazonium salt, its isolation and reaction with aryllithium. The possibility for such transformation results from the relative stability of certain arenediazonium salts such as tetrafluoroborates,[174] hexafluorophosphates,[175, 176] *o*-benzenedisulfonimides,[177, 178] and tosylates.[179]

Tetra-*ortho*-halo(or alkoxy)-substituted azobenzenes **38a – g** can be obtained in two steps. First, *meta*-disubstituted arenes **39a – c** react with n-butyllithium to give the corresponding lithium derivatives **40a – c**, to which arenediazonium salts **41a – d** are added in the next step (Scheme 12).[180]

7.1.6. Coupling of arylhydrazines with aryl halides

Palladium-catalyzed coupling of *N*-Boc-substituted arylhydrazines with aryl halides enables the synthesis of diversely substituted azobenzenes and provides high yields of the products.[181] In photopharmacology, this strategy was employed to prepare a photoswitchable AMPA receptor antagonist **42** (ShuBQX-3) (AMPA is α-amino-3-hydroxy-5-methylisoxazole-4-propionic acid) and its analogues (Scheme 13).[182]

Scheme 13



p-TSA is *para*-toluenesulfonic acid

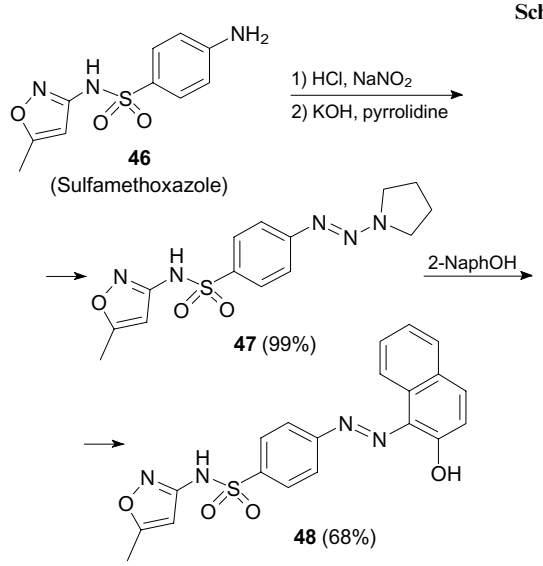
The starting hydrazine **43** containing several functional substituents such as strong electron-withdrawing nitro- and trifluoromethyl groups, and amino and diethylphosphoryl groups, was prepared from phosphonate **44** and *N*-Boc-substituted phenylhydrazine (**45**). The reaction proceeds with the use of standard reagents, namely, palladium acetate and tri(*tert*-butyl)phosphine. The yield of the product **42** is 18% over 3 steps.

7.1.7. Reaction of triazenes with phenols and anilines

Triazenes can be produced *via* the reaction of arenediazonium salts with amines. For example, azo coupling of arenediazonium salts with anilines involves the rearrangement of triazenes to azobenzenes. In some cases, this reaction represents an effective approach to the synthesis of azo compounds.[160]

Presently, triazenes derived from arenediazonium salts and secondary amines are used most often, since such compounds are rather stable and capable of various synthetic transformations including those giving heterocyclic systems.[183] For instance, Zhang *et al.*[184] synthesized a series of azonaphthols *via* this reaction. As starting materials, aryl triazenes, the products of the reaction between arenediazonium salts and pyrrolidine were used, while imidazolium ionic liquids served as promoters. Scheme 14 illustrates an example of the application of this synthetic strategy to post-modification of sulfamethoxazole (**46**), leading *via* triazene **47** to a photoactivated compound **48** in a good yield.

Scheme 14



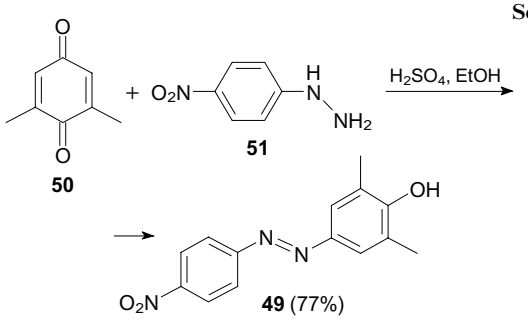
7.1.8. Reaction of quinones with arylhydrazines

The reaction between quinones and arylhydrazines affords azophenols. Reactions of arylhydrazines with synthetic analogues of quinones, quinone acetals, provide azobenzenes bearing methoxy group in the *para*-position relative to the azo group. An example of the use of this strategy is the synthesis of (*E*)-2,6-dimethyl-4-[(4-nitrophenyl)diazenyl]-phenol (**49**) from 2,6-dimethylquinone (**50**) and *p*-nitrophenylhydrazine (**51**) (Scheme 15).[185]

7.1.9. Miscellaneous reactions

Noteworthy is a series of other methods for preparating azobenzenes which can be useful in the synthesis of photopharmacological compounds, namely, reduction of azoxybenzenes, rearrangement of azoxybenzenes into azophenol

Scheme 15



derivatives under the action of Brønsted and Lewis acids (the Wallach reaction), dimerization of arenediazonium salts, thermolysis of aryl azides, ring-opening of benzotriazoles, *etc*. These methods are considered in detail in reviews.[160, 167]

7.2. Methods for the synthesis of bridged azobenzenes

7.2.1. Reductive intramolecular coupling of 1,2-bis(2-nitrophenyl)ethane derivatives

A classic strategy to obtain bridged azobenzenes is reductive intramolecular cross-coupling of 1,2-bis(2-nitrophenyl)-ethane derivatives on treatment with zinc and barium hydroxide followed by oxidation with HgO.[186] For example, dihydrobenzodiazocine **52** intended for modification of proteins was obtained by this method.[187] The sequence of transformations includes the Wittig reaction affording *meta*-nitro-disubstituted stilbene **53** from (3-nitrobenzyl)triphenylphosphonium bromide (**54**) and 3-nitrobenzaldehyde (**55**), the subsequentpalladium-catalyzed hydrogenation, acetylation of 1,2-bis(3-aminophenyl)ethane **56**, and nitration of diacetyl derivative **57**. The final steps include the reductive intramolecular cross-coupling to yield bridged azobenzene **58** bearing amino groups in positions 2 and 9, and their acylation with chloroacetyl chloride (Scheme 16). The disadvantage of this method is the extremely low yield of compound **58**.

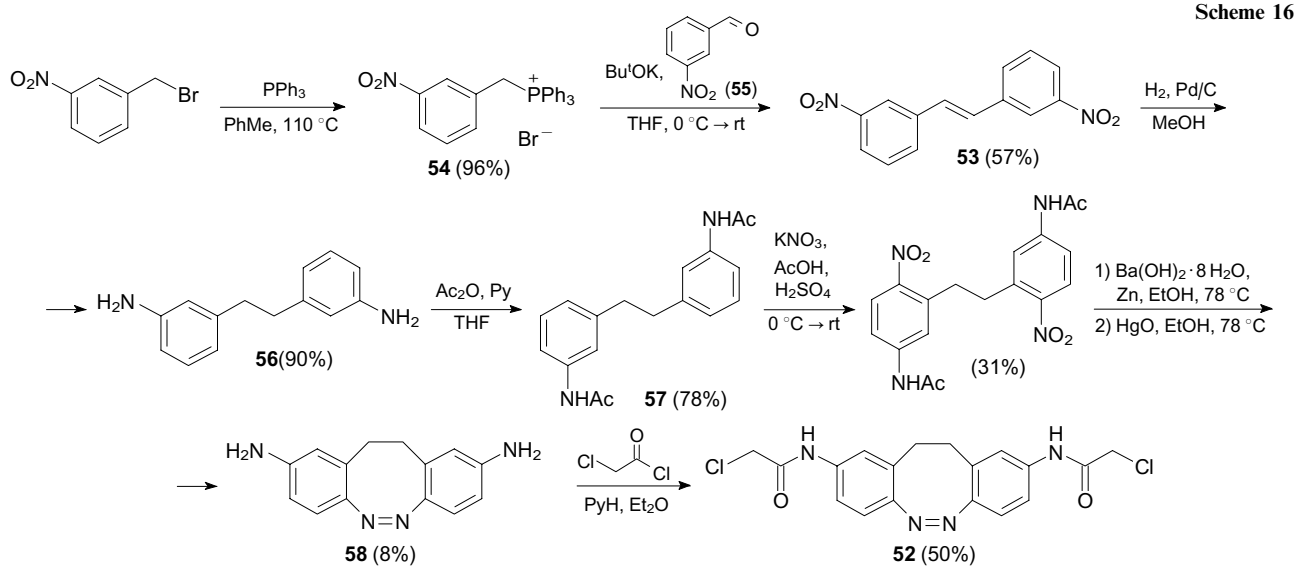
The synthesis of heteroatom-containing dihydrobenzodiazocines has been reported.[83] In the first step, 2-nitrobenzyl bromide (**59**) reacted with 2-nitrophenol (**60**) in the presence of K_3PO_4 and tetra-n-butylamonium bromide (TBAB). Then, the reductive coupling of ether **61** was carried out to give a mixture of isomeric azoxybenzenes **62a**,**b** (44% total yield), which were reduced to dihydrobenzodiazocine **8** (Scheme 17).

To obtain its sulfur-containing analogue **9**, bis(2-nitrophenyl) disulfide (**63**) was reduced with sodium borohydride in the first step, and intermediate thiophenol was allowed to react *in situ* with 2-nitrobenzyl bromide (**59**) to afford the corresponding sulfide **64**. Further transformations were carried out by analogy with those described above for product **8**.

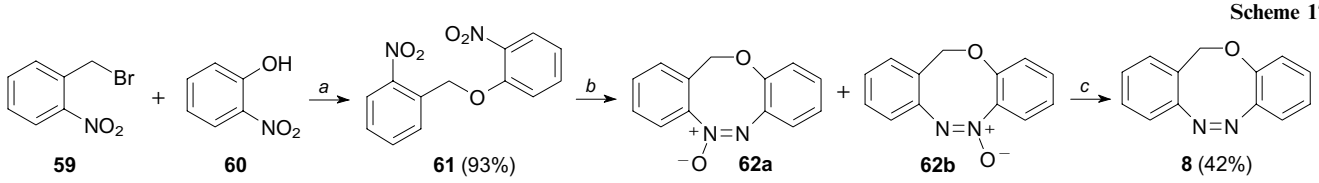
7.2.2. Mills reaction

The Mills reaction can be used as an approach to the synthesis of bridged azobenzenes. For example, Cabré *et al.*[116] recently proposed photoswitchable neurotransmitters for kainate receptors Glu_brAzo 1 (**65a**) and Glu_brAzo 2 (**65b**), containing the bridged azobenzene core. The synthesis of these compounds comprises the preparation of dibromo derivatives of dihydrobenzodiazocine **66**. The photoswitch core is formed by a three-step synthesis: the first step includes the formation of 1,2-bis(4-

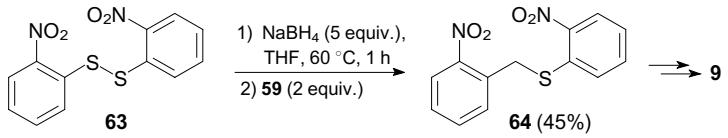
Scheme 16



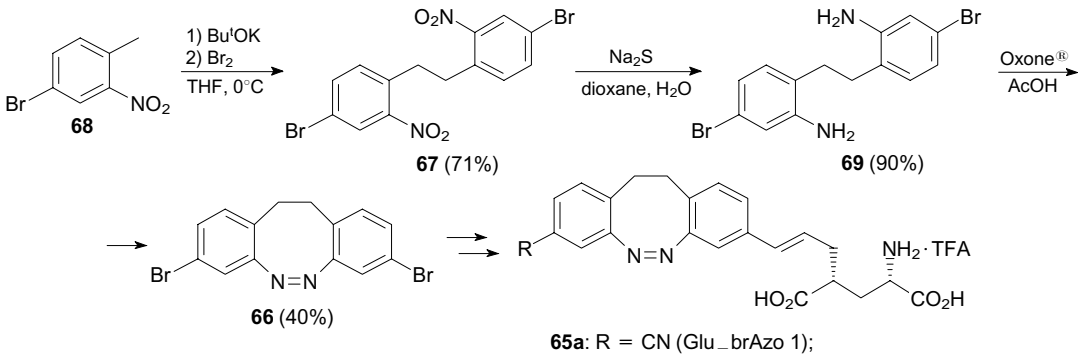
Scheme 17



(*a*) K_3PO_4, TBAB, H_2O; (*b*) Pb, Et_3N, HCO_2H, MeOH, H_2O, pH 9.5, US; (*c*) 1) PPh_3, MoO_2Cl_2; 2) Pb, ball mill (40 Hz), 4 h; US is ultrasound



Scheme 18



TFA is trifluoroacetic acid

bromo-2-nitrophenyl)ethane (**67**) *via* dimerization of 4-bromo-2-nitrotoluene (**68**) induced by potassium *tert*-butoxide and bromine, the second step comprises the reduction of nitro groups to amino groups with sodium sulfide in a dioxane – water mixture (compound **69**), and in the final step, the Mills reaction is carried out using Oxone in glacial acetic acid (Scheme 18).[116]

The resulting transformation can be formally defined as an intramolecular oxidative coupling of anilines in the presence of Oxone as an oxidant; however, the authors have examined the mechanism of this reaction and established that one of the amino groups in compound **69** is oxidized to the nitroso group followed by the intramolecular condensation.

This synthetic approach was also applied to the synthesis of monofunctionalized S-diazocines in yields exceeding those of the classical procedure using lead as a reducing agent.[188]

7.3. Synthesis of azoheteroarenes

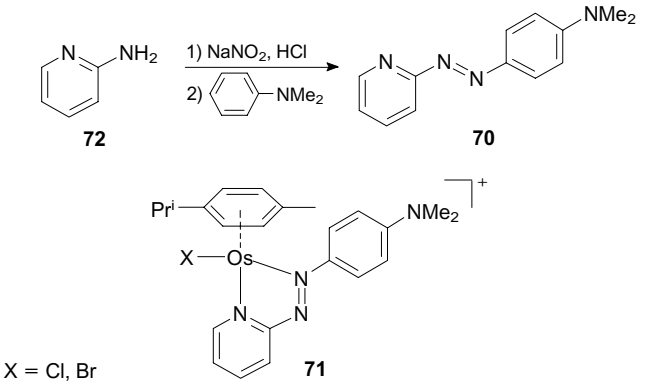
The synthetic strategies towards azoheteroarene photoswitches are dependent on the type of heterocyclic moiety which is a part of the product. To prepare azoheteroarenes comprising azines and their derivatives such as pyridine,

pyrimidine, pyrazine, quinoline, isoquinoline, *etc.*, approaches similar to the synthetic strategies for the substituted azobenzenes are employed. For the synthesis of azoheteroarenes containing five-membered heterocycles with one or several nitrogen, oxygen, and sulfur atoms, a variety of approaches have been elaborated. This is due to the presence of several reaction centres, which can be modified in such molecules, and also to the diversity of the assembly of the heterocyclic moiety.

7.3.1. Azo coupling reaction

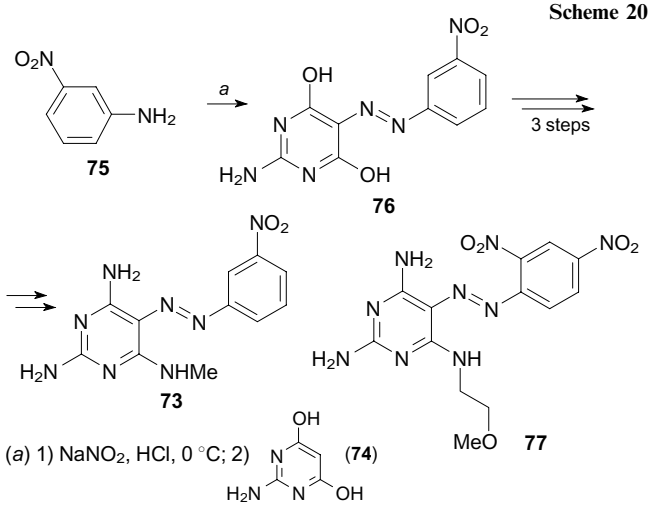
The azo coupling reaction is widely used in the design of azoheteroarenes based on six-membered nitrogen-containing heterocycles and their analogues. For example, Fu *et al.*[189] used this reaction to synthesize ligand **70** for osmium(II) complex **71**, displaying anticancer activity (Scheme 19). This complex can be activated with glutathione, but its main target is the NADH/NAD+ system. By oxidizing NADH to NAD^+, complex **71** violate the cell metabolism, since NADH is found in cells in minor amounts but performs many functions as a coenzyme. *N*,*N*-Dimethyl-4-(2-pyridyldiazenyl)aniline (**70**) is formed through the azo coupling of 2-aminopyridine (**72**) with *N*,*N*-dimethylaniline.

Scheme 19



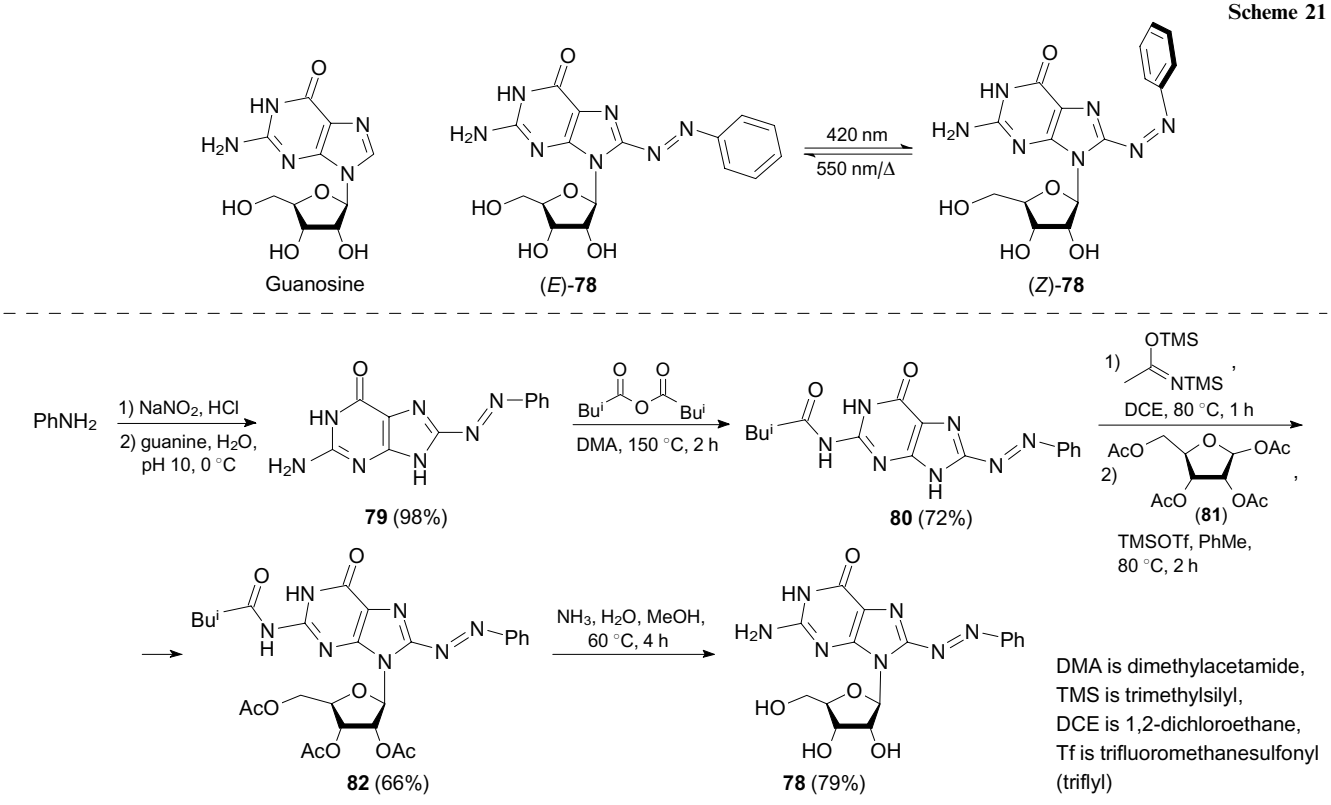
The first step in the synthesis of commercially available 5-azopyrimidine derivative **73** reported by Bártovaá *et al.*[190] is the addition of commercially available 2-amino-4,6-dihydroxypyrimidine (**74**) in an acetate buffer to 3-nitrophenyldiazonium chloride derived from *m*-nitroaniline (**75**). Further modification of the resulting 2-amino-5-[(3-nitrophenyl)diazenyl]pyrimidine-4,6-diol (**76**) leads to the target compound (Scheme 20).

Scheme 20



Similar push-pull azopyrimidines were synthesized the same way by Čechová *et al.*[191] One of the products, arylazopyrimidine **77**, is characterized by a thermal relaxa-

Scheme 21



tion time of 2 ns in methanol and benzene, and its analogue bearing dimethylamino groups in positions 4 and 6 of the pyrimidine ring has a similar relaxation time in benzene.

Azo coupling is an essential reaction opening access to a wide range of azoheteroarenes containing five-membered heterocycles. In this process, π-excessive or π-amphoteric heterocycles, due to their electron-donating properties, often act as azo components. In this way, 2-azoarylpyrroles,[75,192] 3-azoarylpyrroles,[105,192] 2,5-bis(azoarylpyrroles),[193] 3-azoarylpyrroles,[73] 2-azoarylimidazoles,[194–197] 5-azoaryloxazoles,[198] 2-arylazobenzimidazoles,[199] 3-azothiophens,[200] and some other azoheteroarenes were obtained.

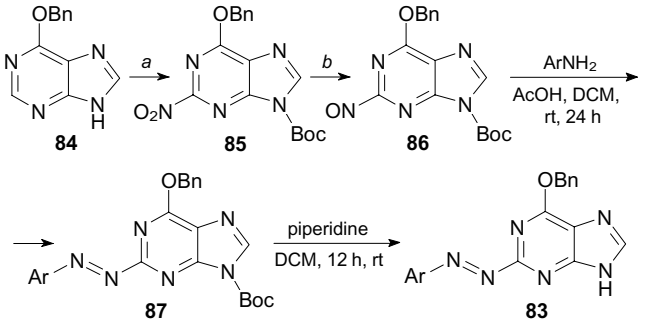
This reaction can also give rise to 2-azoheteroarenes if binuclear heterocycles containing several nitrogen atoms are used as azo components. For example, a photochromic derivative of guanosine, 8-(phenyldiazenyl)guanosine (**78**), capable of photoisomerizing under visible violet and green light irradiation, was prepared from aniline in several steps. First, benzenediazonium salt generated by aniline diazotization was coupled with guanine to yield an azo derivative **79**. Further modification of the latter compound included several steps, necessary to the introduction of the ribose residue.[201] 2-Amino group in compound **79** was protected with the acyl group, and then the coupling reaction between intermediate **80** and tetraacetylated ribose (**81**) was carried out. The final step included the total deprotection of compound **82** in a basic medium (Scheme 21).

7.3.2. Mills reaction

To prepare azoheteroarenes *via* the Mills reaction, condensation of arylamines with nitroso hetarenes, hetarylamines with nitroso arenes, or hetarylamines with nitroso hetarenes can be carried out. To choose a synthetic strategy, several factors should be taken into account, including the stability of the starting compounds. The Mills reaction can be utilized to prepare azoheteroarenes, which are unavailable or hard-to-reach for the azo coupling reaction, such as 3-azoarylpyrazoles, 5-azoarylpyrazoles, azoaryltetrazoles, 3-azoaryl-1,2,4-triazoles, *etc*.[105]

For example, this reaction was used to modify position 2 in the purine ring. A series of arylazopurines **83** was thus synthesized, which were tested as photoisomerizable inhibitors of O^6-alkylguanine-DNA.[202] The reaction sequence included protection of the pyrrole nitrogen atom of guanine **84** with Boc-protecting group, nitration of *N*-Boc-guanine **85** under mild conditions with the further reduction of the nitro group to the nitroso one, condensation of 2-nitrosoguanine derivative **86** with various anilines, and Boc-deprotection of compound **87** (Scheme 22).

Scheme 22

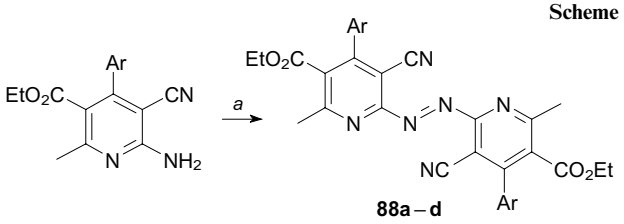


(*a*) 1) Boc_2O, DMAP, DCM, rt, 16 h; 2) TBAN, TFAA, DCM, 0 °C, 1 h; (*b*) 1) 10 mol.% Pt/C H_2 (1 atm), EtOAc, MeOH, AcOH, rt, 0.5 h; 2) $NaIO_4$, DCM, H_2O, 0 °C, 2 h; DMAP is 4-dimethylaminopyridine, TBAN is tetra-n-butylammonium nitrate, TFAA is trifluoroacetic anhydride

7.3.3. Oxidative coupling of hetarylamines

Oxidative coupling of hetarylamines is used to prepare symmetrical azoheteroarenes. Da Silve *et al*.[72] proposed a synthetic approach to obtain symmetrical azopyridines **88a–d**, bearing various substituents in the ring, and *N*-methylated cyano-substituted azopyrazoles. The *N*-bromosuccinimide–benzoyl peroxide system was employed (Scheme 23).

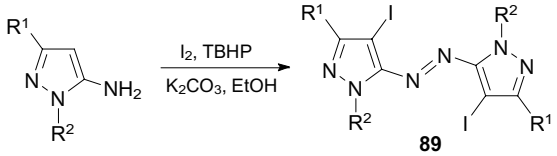
Scheme 23



(*a*) NBS, $(PhCO)_2O_2$, MeCN, Δ;
Ar = Ph (**a**, 79%), 4-ClC_6H_4 (**b**, 68%), 2-MeC_6H_4 (**c**, 74%), 4-Py (**d**, 40%); NBS is *N*-bromosuccinimide

Klapötke and Piercey[203] used sodium dichloroisocyanurate as an oxidant to obtain 1,1′-azobis(tetrazoles). Jiang *et al*.[204] implemented this reaction to synthesize symmetrical 5-azopyrazoles. When utilizing CuI–*tert*-butyl hydroperoxide (TBHP) oxidizing system in the presence of phenanthrolines, usual azopyrazoles were isolated. With I_2–TBHP oxidizing system, the simultaneous iodination of position 2 occurred leading to azopyrazole iodo-derivatives **89**, which are convenient reagents for further modifications, *e.g*., for the Sonogashira cross-coupling (Scheme 24).

Scheme 24

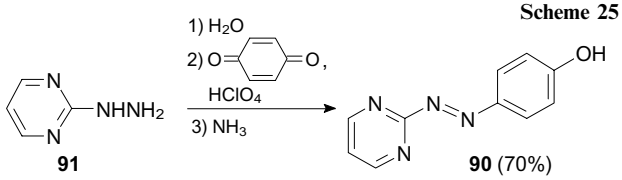


R^1 = H: R^2 = Me (48%), Et (61%); R^1 = Me: R^2 = Ph (86%), Me (66%), 4-MeC_6H_4 (64%); R^1 = Bu^t, R^2 = Ph (68%); R^1 = cyclo-C_3H_5: R^2 = Me (70%), Ph (69%); R^1 = Ph, R^2 = 4-BrC_6H_4 (77%); R^1 = 4-MeC_6H_4, R^2 = Ph (83%); R^1 = 4-ClC_6H_4, R^2 = Me (89%)

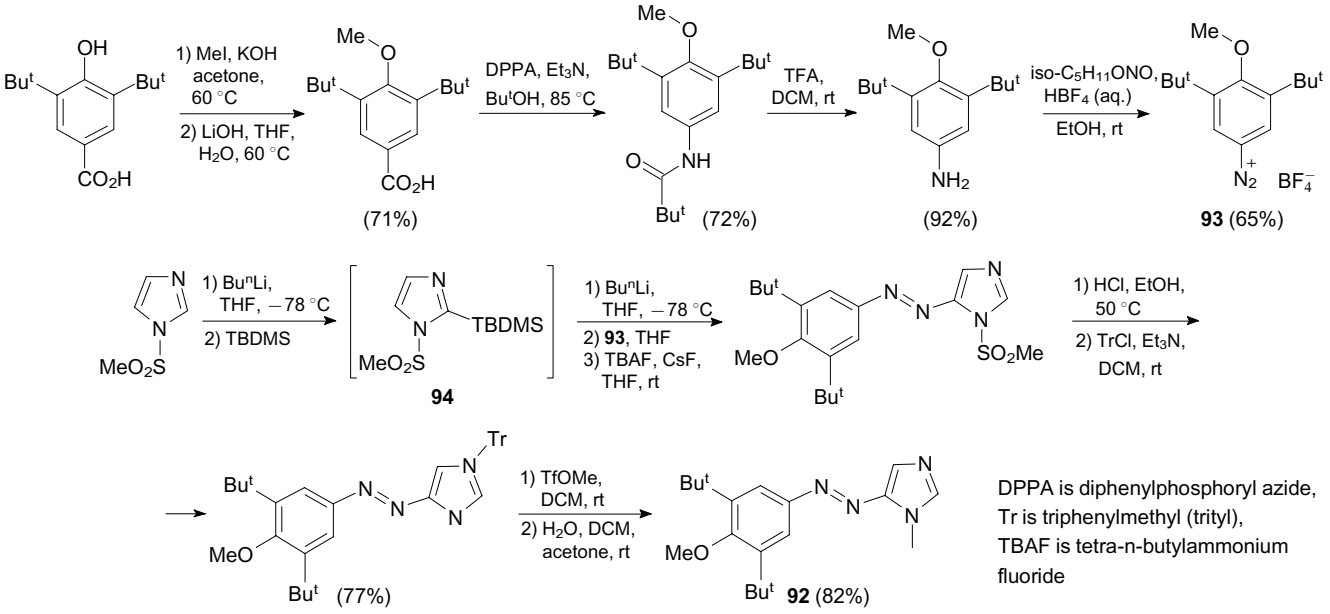
7.3.4. Reactions of quinones with arylhydrazines

The title reaction used in the synthesis of azophenols can be applied to obtain azoheteroarenes. For example, (pyrimi-

Scheme 25



Scheme 26



din-2-yl)azophenol **90**, soluble in a sodium phosphate buffer and having a thermal relaxation rate of 40 ns in a phosphate buffer at pH 7.8, was obtained by this reaction from pyrimidine-2-hydrazine (**91**) and 1,4-benzoquinone (Scheme 25).[69]

7.3.5. Coupling of arenediazonium salts with hetaryl lithium derivatives

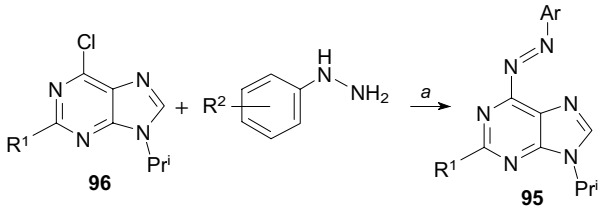
Coupling of arenediazonium salts with hetaryl lithium derivatives is directed at producing azoheteroarenes, which are hard-to-reach *via* the azo coupling reaction, for example, imidazoles bearing aryldiazenyl group in position 5. This synthesis is exemplified in a study[205] describing 5-arylazoimidazole **92** and its analogues. These compounds are photodissociable ligands of the nickel porphyrin complex, changing its spin state through light-induced coordination – dissociation. More stable *E*-isomer coordinates to the complex, while *Z*-isomer dissociates due to the steric repulsion. The synthesis of compound **92** includes the coupling reaction between arenediazonium tetrafluoroborate **93** and the corresponding 5-lithioimidazole generated *in situ* from 2-(*tert*-butyldimethylsilyl)-1-(methanesulfonyl)-1*H*-imidazole (**94**) protected in positions 1 and 2. Methanesulfonyl and *tert*-butyldimethylsilyl (TBDMS) groups served as protecting functions. The reactions employed to obtain salt **93** are illustrated in Scheme 26.

7.3.6. Coupling of arylhydrazines with hetaryl halides with the subsequent oxidation

Azoheteroarenes can be produced *via* palladium-catalyzed cross-coupling of hetaryl halides with *N*-Boc-*N*-phenylhydrazines and the subsequent oxidation with oxygen under microwave (MW) irradiation. This approach provided the synthesis of derivatives of 3-azopyridine, 5-azopyrimidine, 3-azoquinoline, 5-azoindole, 5-azopyrrolo[2,3-*b*]pyridine, and 3-azoindazole in good yields.[206]

Recently, Kolarski *et al.*[207] obtained 6-azopurines **95** *via* the two-step one-pot microwave-assisted synthesis from aryl hydrazines and substituted 6-chloropurines **96** (Scheme 27) in the absence of palladium catalysis. The authors synthe-

Scheme 27



(*a*) 1) DIPEA, ButnOH, 150 – 180 °C, MW, 1 – 3 h; 2) O_2, 0.5 – 24 h;
R^1 = H: Ar = Ph (98%), 4-MeC_6H_4 (98%), 4-$MeOC_6H_4$ (86%), 4-FC_6H_4 (92%), 4-NCC_6H_4 (98%), 4-$HO_2CC_6H_4$ (89%), 3-FC_6H_4 (93%), 3-NCC_6H_4 (87%), 3-ClC_6H_4 (99%), 3-MeC_6H_4 (93%), 3-$HO_2CC_6H_4$ (98%), 3,5-$Cl_2C_6H_3$ (92%), 3,5-$F_2C_6H_3$ (93%), 2,6-$Cl_2C_6H_3$ (91%), 2,6-$Me_2C_6H_3$ (91%), 2-Naph (96%), 2,5-$Cl_2C_6H_3$ (95%), 2,4,6-$F_3C_6H_2$ (85%); R^1 = NH_2: Ar = 4-NCC_6H_4 (87%), 4-FC_6H_4 (99%), Ph (85%), 3-ClC_6H_4 (90%), 3-FC_6H_4 (92%), 3,5-$Cl_2C_6H_3$ (97%), 3,5-$F_2C_6H_3$ (83%), 2-Naph (95%); DIPEA is diisopropylethylamine

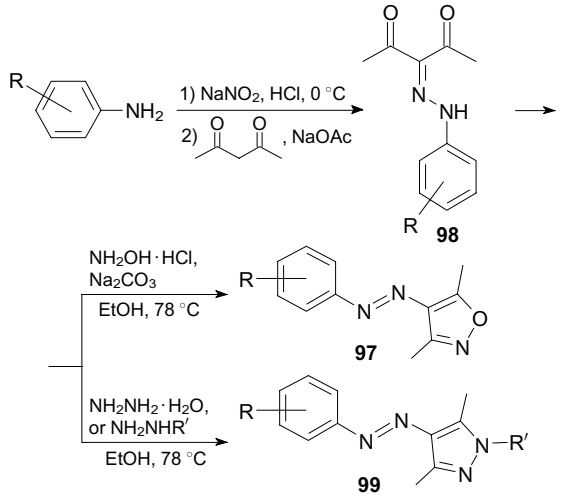
sized 18 azoadenine derivatives (R^1 = H) and 8 azoguanines (R^1 = NH_2). The absorption maxima in these spectra of these compounds appear in the range from 420 to 480 nm.

7.3.7. Heterocycle assembly

Kumar *et al.*[208] described 4-arylazoisoxazoles **97**, having demonstrated good photochemical characteristics. The first synthetic step includes the reaction of arene diazonium salt, obtained by diazotization of various anilines, with acetylacetone. Then the intermediate hydrazones **98** are condensed with hydroxylamines in a basic system to afford the target compounds. Apart from substituted arylazoisoxazoles, this reaction provided a hetero analogue of these compounds, namely, 3,5-dimethyl-4-(3-pyridyldiazenyl)-isoxazole (78% yield).

The reaction of hydrazone **98** with methylhydrazine or hydrazine hydrate was reported[75,209] to afford switches promising for photopharmacology, namely, 4-azoarylpyrazole derivatives **99**. Weston *et al.*[210] used this transforma-

Scheme 28

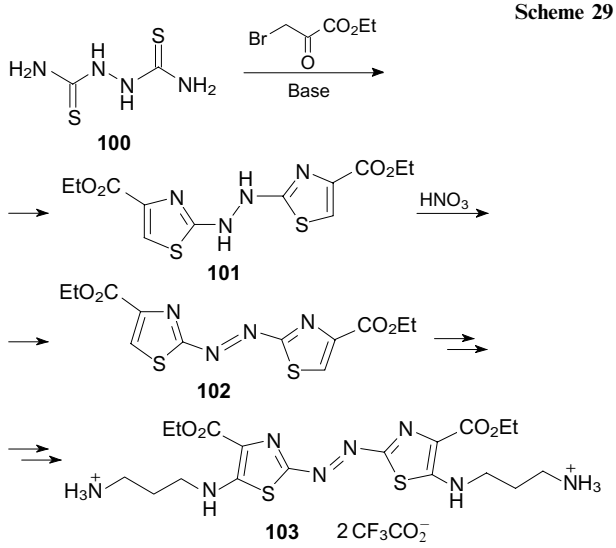


97: R = H (85%), 2-F (96%), 3-F (89%), 4-F (50%), 2-Cl (54%), 3-Cl (84%), 4-Cl (85%), 2-Br (67%), 3-Br (72%), 4-Br (75%), 4-I (94%), 2-OH (93%), 3-OH (71%), 4-OH (79%), 3-CF_3 (89%), 4-CF_3 (62%), 2-OMe (78%), 3-OMe (75%), 4-OMe (80%), 2-NO_2 (60%), 4-NO_2 (97%), 4-Me (87%), 3-NHAc (82%), 4-NHAc (80%), benzo[3,4] (78%), 2,5-Cl_2 (54%), 2,6-Cl_2 (71%), 2,4-F_2 (78%), 2,5-F_2 (54%), 2,6-F_2 (53%), 3,5-F_2 (87%), 2-NH_2 (78%), 3-NH_2 (82%), 4-NH_2 (73%), 2-CN (51%), 4-(N═N-Ph) (69%);
99: R′ = H: R = H (~100%), 2,6-F_2 (~100%), 4-OH (~100%); R = H, R′ = Me (~100%); R = 4-I: R′ = Me (92%), R′ = Bn (68%), R′ = 2-Naph (14%)

tion to synthesize 4-azoarylpyrazoles having optimal characteristics.

Pithan *et al.*[211] reported the synthesis of 5-alkyl- and 5-phenylamino-substituted azothiazole dyes displaying solvatochromic and DNA-binding properties. The symmetric azothiazole backbone was built with the use of the modified Hantzsch reaction. 2,5-Dithiobisurea **100** was condensed with ethyl 3-bromopyruvate to give symmetrical hydrazine **101**, which was oxidized with cold nitric acid to symmetrical azothiazole **102**. The subsequent two-step modification led to target compound **103** (Scheme 29).

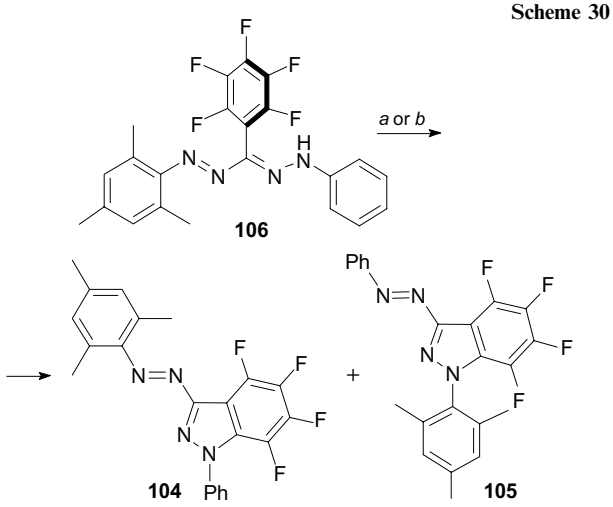
Scheme 29



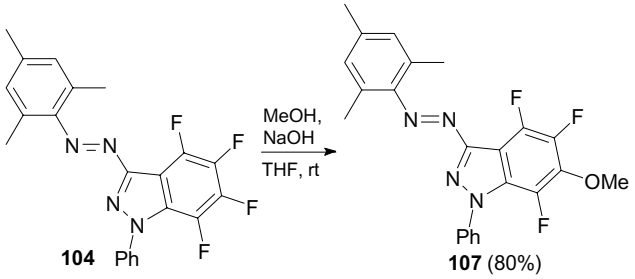
7.3.8. Miscallaneous methods for the synthesis of azoheteroarenes

Travieso-Puente *et al.*[212] prepared 3-arylazoindazoles **104**, **105** *via* aromatic nucleophilic substitution in the presence of strong bases such as potassium hydride. Pentafluorophenyl-containing formazan **106** was used as a starting material. 3-Arylazoindazole **104** can undergo further nucleophilic substitution in aromatic groups to afford, *e.g.*, compound **107** (Scheme 30). The products possess high photostability and long lifetimes of the *Z*-isomer.

Scheme 30



(*a*) $ZnMe_2$, PhMe, 80 – 130 °C (54%, **104** : **105** = 10 : 1);
(*b*) KH, THF, rt (94%, **104** : **105** = 1.45 : 1)



8. Conclusion

Currently, photopharmacology is at the very early stage of its development; preliminary studies have shown that the use of photopharmacological compounds in medical practice has great potential. To achieve this aim, several tasks must be addressed, including the search for effective photoswitches for use as a part of a photopharmacological drug; elaboration of approaches to the design and synthesis of such compounds based on classical pharmaceutical drugs and photoswitches; adaptation of known methods of photodynamic therapy to photopharmacology, their modification and optimization; development of methodologies for testing drugs *in vivo* in animal models, *etc.*

In most publications reported to date, the authors used a simple strategy for designing a photopharmacological drug based on two components, namely, a molecular photoswitch and a biologically active compound. However, such a strategy can be useful only in the early stage of the design and rarely produces the final drug without additional modifications. The further development of photopharmacology requires more intensive involvement of classical

methods and approaches used in the development of classical pharmaceuticals,[6] which imply screening of libraries of compounds and optimization of not only biological activity but also other physicochemical characteristics. Thus, the rational design of photopharmacological compounds requires optimization of the spectral and photochemical properties of the drug.

Currently, about a dozen molecular switches of various types are known, which can find application in photopharmacology, and also other potential photoswitches, including photoactive amino acids and nucleotides. It should be noted that in recent years, there has been a tendency to use azoheteroarenes, rather than azobenzenes, as photoactive parts of the drug, due to their high biological activity. However, as apparent from the present review, for the design of azoheteroarene-based molecular photoswitches, along with specific approaches, strategies developed for azobenzene derivatives are actively used. Thus, the basic principles of molecular design presented here, computational modelling methods, and synthetic approaches to the photopharmacological switches based on azobenzenes and azoheteroarenes can be useful for the further development of this promising field of chemistry.

This review was financially supported by the Russian Foundation for Basic Research (Project No. 19-115-50477 Expansion) and 5 – 100 Russian Federation programme in the Peter the Great St. Petersburg Polytechnic University.

9. List of acronyms and designations

AMPA — α-amino-3-hydroxy-5-methylisoxazole-4-propionic acid,
Boc — *tert*-butoxycarbonyl,
CASPT2 — complete active space second order perturbation theory
CCSD(T) — coupled cluster singles and doubles (triples) excitations,
m-CPBA — *m*-chloroperoxobenzoic acid,
DBU — diazabicyclo[5.4.0]undec-7-ene,
DCE — 1,2-dichloroethane,
DCM — dichloromethane,
DFT — density functional theory,
DIPEA — diisopropylethylamine,
DMA — dimethylacetamide,
DMAP — 4-dimethylaminopyridine,
DPPA — diphenylphosphoryl azide,
EC_{50} — drug concentration which can induce a response equal to 50% of the maximum effect,
GABA — γ-aminobutyric acid,
HOMO — highest occupied molecular orbital,
LPA — lysophosphatidic acid (receptors),
LUMO — lowest unoccupied molecular orbital,
MNPs — magnetic nanoparticles,
MP2 — second-order Moller – Plesset perturbation theory,
MRCI — multireference configuration interaction,
MW — microwave irradiation,
NADH and NAD^+ — reduced and oxidized forms of nicotinamide adenine dinucleotide,
Naph — naphthyl,
NBS — *N*-bromosuccinimide,
NCS — *N*-chlorosuccinimide,
NEVPT2 — second order N-electron valence state perturbation theory,
PCC — pyridinium chlorochromate,
PCM — polarizable continuum model,
Py — pyridyl,
rt — room temperature,
QM/MM — quantum mechanics/molecular mechanics,
RASPT2 — second-order restricted active space second order perturbation theory,
TBAB — tetra-n-butylammonium bromide,
TBAF — tetra-n-butylammonium fluoride,
TBAN — tetra-n-butylammonium nitrate,
TBDMS — *tert*-butyldimethylsilyl,
TBHB — *tert*-butyl hydroperoxide,
TD-DFT – time-dependent density functional theory,
Tf — trifluoromethanesulfonyl (triflyl),
TFA — trifluoroacetic acid,
TFAA — trifluoroacetic anhydride,
TMS — trimethylsilyl,
Tr — triphenylmethyl (trityl),
TRPV1 — transient receptor potential cation channel subfamily V member 1,
p-TSA — *p*-toluenesulfonic acid,
US — ultrasound,
ΔE_{rel} — energy difference,
ΔG — Gibbs energy difference between *Z*- and *E*-isomers,
ε — molar absorption coefficient,
Γ – conversion rate (the content of the resulting isomer) upon irradiation of the compound at the certain wavelength,
λ_{max} — maximum absorption wavelength,
λ_{ex} — photoexcitation wavelength (light-emitting diode),
Φ — quantum yield.

References

1. K.Hüll, J.Morstein, D.Trauner. *Chem. Rev.*, **118**, 10710 (2018)
2. M.M.Lerch, M.J.Hansen, G.M.van Dam, W.Szymanski, B.L.Feringa. *Angew. Chem., Int. Ed.*, **55**, 10978 (2016)
3. P.Brezhestovskii, G.Maleeva. *Zh. Vyssh. Nerv. Deyat.*, **67** (5) , 41 (2017)
4. P.Bregestovski, G.Maleeva. *Neurosci. Behav. Physiol.*, **49**, 184 (2019)
5. J.Morstein, D.Trauner. *Curr. Opin. Chem. Biol.*, **50**, 145 (2019)
6. M.J.Fuchter. *J. Med. Chem.*, **63**, 11436 (2020)
7. P.Leippe, J.Koehler Leman, D.Trauner. *Biochemistry*, **56**, 5214 (2017)
8. D.M.Nikolaev, M.S.Panov, A.A.Shtyrov, V.M.Boitsov, (S.Y.Vyazmin, O.B.Chakchir, I.P.Yakovlev, M.N.Ryazantsev. In *Progress in Photon Science*. (Eds K.Yamanouchi, S.Tunik, V.Makarov). (Springer, 2019). P. 139
9. M.N.Khan, D.K.Parmar, D.Das. *Mini-Rev. Med. Chem.*, **21**, 380 (2020)
10. I.M.Welleman, M.W.Hoorens, B.L.Feringa, H.H.Boersma, W.Szymański. *Chem. Sci.*, **11**, 11672 (2020)
11. J.A.Frank, M.-J.Antonini, P.-H.Chiang, A.Canales, D.Konrad, I.Garwood, G.Rajic, F.Koehler, Y.Fink, P.Anikeeva. *ACS Chem. Neurosci.*, **11**, 3802 (2020)

12. S.Berlin, E.Y.Isacoff. In *Handbook of Neurophotonics*. (Eds F.S.Pavone, S.Shoham). (Boca Raton, FL: CRC Press, 2020). P. 271
13. W.Li, R.M.Elhassan, H.Fang, X.Hou. *Future Sci.*, **12**, 1991 (2020)
14. M.Scheiner, A.Sink, P.Spatz, E.Endres, M.Decker. *ChemPhotoChem*, **4**, 1 (2020)
15. A.E.Berizzi, C.Goudet. In *From Structure to Clinical Development: Allosteric Modulation of G Protein-Coupled Receptors*. (*Ser. Advances in Pharmacology*. Vol. 88). (Ed. C.Langmead). (Elsevier, 2020). P. 143
16. M.M.Shchepinova, A.C.Hanyaloglu, G.S.Frost, E.W.Tate. *Curr. Opin. Chem. Biol.*, **56**, 98 (2020)
17. A.Acosta-Ruiz, V.A.Gutzeit, M.J.Skelly, S.Meadows, J.Lee, P.Parekh, A.G.Orr, C.Liston, K.E.Pleil, J.Broichhagen. *Neuron*, **105**, 446 (2020)
18. P.Paoletti, G.C.Ellis-Davies, A.Mourot. *Nat. Rev. Neurosci.*, **20**, 514 (2019)
19. A.Damijonaitis, D.M.Barber, D.Trauner. *Neurotransmitter*, **3**, e1292 (2016)
20. D.Lemoine, S.Mondoloni, J.Tange, B.Lambolez, P.Faure, A.Taly, L.Tricoire, A.Mourot. *Elife*, **9**, e59026 (2020)
21. N.Hartrampf, T.Seki, A.Baumann, P.Watson, N.A.Vepřek, B.E.Hetzler, A.Hoffmann-Röder, M.Tsuji, D.Trauner. *Chem. – Eur. J.*, **26**, 4476 (2020)
22. A.S.Lubbe, W.Szymanski, B.L.Feringa. *Chem. Soc. Rev.*, **46**, 1052 (2017)
23. F.Iseppon, M.Arcangeletti. *STEMedicine*, **1**, e43 (2020)
24. P.Gazerani. *Future Medicine*, **7**, 341 (2017)
25. Y.Q.Yeoh, J.R.Horsley, J.Yu, S.W.Polyak, B.Jovcevski, A.D.Abell. *ChemMedChem*, **15**, 1505 (2020)
26. J.Morstein, J.B.Trads, K.Hinnah, S.Willems, D.M.Barber, M.Trauner, D.Merk, D.Trauner. *Chem. Sci.*, **11**, 429 (2020)
27. M.N.Pinto, P.K.Mascharak. *J. Photochem. Photobiol. C*, **42**, 100341 (2020)
28. D.A.Rodríguez-Soacha, M.Decker. *Adv. Ther.*, **1**, 1800037 (2018)
29. A.Y.Rotov, L.Astakhova, V.Sitnikova, A.Evdokimov, V.Boitsov, M.Dubina, M.Ryazantsev, M.Firsov. *Acta Naturae*, **10**, 75 (2018)
30. S.Kleinlogel, C.Vogl, M.Jeschke, J.Neef, T.Moser. *Physiol. Rev.*, **100**, 1467 (2020)
31. A.Y.Vorobev, A.E.Moskalensky. *Comput. Struct. Biotechnol. J.*, **18**, 27 (2020)
32. L.Josa-Culleré, A.Llebaria. *ChemPhotoChem*, **4**, e1 (2020)
33. C.Hoppmann, L.Wang. In *Methods in Enzymology*. (Elsevier, 2019). P. 249
34. O.N.Zefirova, N.S.Zefirova. *Vestn. MGU. Ser. 2, Khimiya (Bull. Moscow State Univ., Ser. 2, Chem.)*, **41**, 43 (2000)
35. O.N.Zefirova, N.S.Zefirova. *Vestn. MGU. Ser. 2, Khimiya* (*Bull. Moscow State Univ., Ser. 2, Chem.)*, **41**, 103 (2000)
36. I.I.Baskin, V.A.Palyulin, N.S.Zefirov. *Russ. Chem. Rev.*, **78**, 495 (2009)
37. *Drug Bioavailability: Estimation of Solubility, Permeability, Absorption and Bioavailability. (Ser. Methods and Principles in Medicinal Chemistry*. Vol. 40). (Eds H.van de Waterbeemd, B.Testa). (2nd Edn). (Wiley-VCH, 2009)
38. *Drug Design Strategies: Quantitative Approaches*. (Eds D.J.Livingstone, A.M.Davis). (Cambridge: Royal Society of Chemistry, 2011)
39. E.Stevens. *Medicinal Chemistry: the Modern Drug Discovery Process*. (Pearson, 2014)
40. S.Crespi, N.A.Simeth, B.König. *Nat. Rev. Chem.*, **3**, 133 (2019)
41. M.Dong, A.Babalhavaeji, M.Hansen, L.Kalman, G.Woolley. *Chem. Commun.*, **51**, 12981 (2015)
42. D.Bleger, S.Hecht. *Angew. Chem., Int. Ed.*, **54**, 11338 (2015)
43. H.D.Bandara, S.C.Burdette. *Chem. Soc. Rev.*, **41**, 1809 (2012)
44. A.A.Beharry, O.Sadovski, G.A.Woolley. *J. Am. Chem. Soc.*, **133**, 19684 (2011)
45. C.A.Lipinski, F.Lombardo, B.W.Dominy, P.J.Feeney. *Adv. Drug Deliv. Rev.*, **23**, 3 (1997)
46. L.Vetráková, V.Ladányi, J.Al Anshori, P.Dvořák, J.Wirz, D.Heger. *Photochem. Photobiol. Sci.*, **16**, 1749 (2017)
47. P.Birnbaum, J.Linford, D.Style. *J. Chem. Soc., Faraday Trans.*, **49**, 735 (1953)
48. H.Rau. *Angew. Chem., Int. Ed. Engl.*, **12**, 224 (1973)
49. A.A.Beharry, G.A.Woolley. *Chem. Soc. Rev.*, **40**, 4422 (2011)
50. V.Ladányi, P.Dvořák, J.Al Anshori, L.Vetráková, J.Wirz, D.Heger. *Photochem. Photobiol. Sci.*, **16**, 1757 (2017)
51. L.Yu, C.Xu, C.Zhu. *Phys. Chem. Chem. Phys.*, **17**, 17646 (2015)
52. E.Fischer. *J. Am. Chem. Soc.*, **82**, 3249 (1960)
53. A.Cembran, F.Bernardi, M.Garavelli, L.Gagliardi, G.Orlandi. *J. Am. Chem. Soc.*, **126**, 3234 (2004)
54. G Lewis. *J. Org. Chem.*, **25**, 2193 (1960)
55. J.Garcia-Amorós, S.Nonell, D.Velasco. *Chem. Commun.*, **48**, 3421 (2012)
56. H.Jaffe, S.-J.Yeh, R.Gardner. *J. Mol. Spectrosc.*, **2**, 120 (1958)
57. Y.Nomura, H.Anzai, R.Tarao, K.Shiomi. *Bull. Chem. Soc. Jpn.*, **37**, 967 (1964)
58. N.Nishimura, T.Sueyoshi, H.Yamanaka, E.Imai, S.Yamamoto, S.Hasegawa. *Bull. Chem. Soc. Jpn.*, **49**, 1381 (1976)
59. J.Olmsted III, J.Lawrence, G.G.Yee. *Sol. Energy*, **30**, 271 (1983)
60. A.Albini, E.Fasani, S.Pietra. *J. Chem. Soc., Perkin Trans.*, 1021 (1983)
61. R.Tahara, T.Morozumi, H.Nakamura, M.Shimomura. *J. Phys. Chem. B*, **101**, 7736 (1997)
62. A.A.Blevins, G.Blanchard. *J. Phys. Chem. B*, **108**, 4962 (2004)
63. P.Sierocki, H.Maas, P.Dragut, G.Richardt, F.Vögtle, L.De Cola, F.Brouwer, J.I.Zink. *J. Phys. Chem. B*, **110**, 24390 (2006)
64. Q.Ya, X.-Z.Dong, W.-Q.Chen, X.-M.Duan. *Dyes Pigm.*, **79**, 159 (2008)
65. G.Gabor, E.Fischer. *J. Phys. Chem.*, **75**, 581 (1971)
66. S.Kobayashi, H.Yokoyama, H.Kamei. *Chem. Phys. Lett.*, **138**, 333 (1987)
67. J.Garcia-Amorós, M.C.R.Castro, P.Coelho, M.M.M.Raposo, D.Velasco. *Chem. Commun.*, **49**, 11427 (2013)
68. J.Garcia-Amoros, W.A.Massad, S.Nonell, D.Velasco. *Org. Lett.*, **12**, 3514 (2010)
69. J.Garcia-Amorós, M.Díaz-Lobo, S.Nonell, D.Velasco. *Angew. Chem., Int. Ed.*, **51**, 12820 (2012)
70. A.G.Gilani, M.Moghadam, M.Zakerhamidi, E.Moradi. *Dyes Pigm.*, **92**, 1320 (2012)

71. E.Procházková, L.Čechová, J.Kind, Z.Janeba, C.M.Thiele, M.Dračínský. *Chem. – Eur. J.* **24**, 492 (2018)
72. D.B.da Silva, A.Samadi, L.Infantes, M.do Carmo Carreiras, J.Marco-Contelles. *Tetrahedron Lett.*, **51**, 6278 (2010)
73. N.A.Simeth, S.Crespi, M.Fagnoni, B.König. *J. Am. Chem. Soc.*, **140**, 2940 (2018)
74. S.Ludwanowski, M.Ari, K.Parison, S.Kalthoum, P.Straub, N.Pompe, S.Weber, M.Walter, A.Walther. *Chem. – Eur. J.*, **26**, 13203 (2020)
75. C.E.Weston, R.D.Richardson, P.R.Haycock, A.J.White, M.J.Fuchter. *J. Am. Chem. Soc.*, **136**, 11878 (2014)
76. G.Féraud, C.Dedonder-Lardeux, C.Jouvet, E.Marceca. *J. Phys. Chem. A*, **120**, 3897 (2016)
77. M.S.Scholz, J.N.Bull, N.J.Coughlan, E.Carrascosa, B.D.Adamson, E.J.Bieske. *J. Phys. Chem. A*, **121**, 6413 (2017)
78. S.Samanta, A.Babalhavaeji, M.X.Dong, G.A.Woolley. *Angew. Chem., Int. Ed.*, **52**, 14127 (2013)
79. M.Dong, A.Babalhavaeji, C.V.Collins, K.Jarrah, O.Sadovski, Q.Dai, G.A.Woolley. *J. Am. Chem. Soc.*, **139**, 13483 (2017)
80. C.E.Weston, R.D.Richardson, M.J. Fuchter. *Chem. Commun.*, **52**, 4521 (2016)
81. R.Siewertsen, H.Neumann, B.Buchheim-Stehn, R.Herges, C.Näther, F.Renth, F.Temps. *J. Am. Chem. Soc.*, **131**, 15594 (2009)
82. L.Heintze, D.Schmidt, T.Rodat, L.Witt, J.Ewert, M.Kriegs, R.Herges, C.Peifer. *Int. J. Mol. Sci.*, **21**, 8961 (2020)
83. M.Hammerich, C.Schütt, C.Stähler, P.Lentes, F.Röhricht, R.Höppner, R.Herges. *J. Am. Chem. Soc.*, **138**, 13111 (2016)
84. P.Lentes, E.Stadler, F.Röhricht, A.Brahms, J.Gröbner, F.D.Sönnichsen, G.Gescheidt, R.Herges. *J. Am. Chem. Soc.*, **141**, 13592 (2019)
85. C.L.Forber, E.C.Kelusky, N.J.Bunce, M.C.Zerner. *J. Am. Chem. Soc.*, **107**, 5884 (1985)
86. H.Bisle, H.Rau. *Chem. Phys. Lett.*, **31**, 264 (1975)
87. D.Bléger, J.Schwarz, A.M.Brouwer, S.Hecht. *J. Am. Chem. Soc.*, **134**, 20597 (2012)
88. L.N.Lameijer, S.Budzak, N.A.Simeth, M.J.Hansen, B.L.Feringa, D.Jacquemin, W.Szymanski. *Angew. Chem.*, **132**, 21847 (2020)
89. C.Boulègue, M.Löweneck, C.Renner, L.Moroder. *ChemBioChem*, **8**, 591 (2007)
90. E.M.Kosower, H.Kanety-Londner. *J. Am. Chem. Soc.*, **98**, 3001 (1976)
91. S.Samanta, T.M.McCormick, S.K.Schmidt, D.S.Seferos, G.A.Woolley. *Chem. Commun.*, **49**, 10314 (2013)
92. L.Albert, A.Peñalver, N.Djokovic, L.Werel, M.Hoffarth, D.Ruzic, J.Xu, L.O.Essen, K.Nikolic, Y.Dou. *ChemBioChem*, **20**, 1417 (2019)
93. O.Sadovski, A.A.Beharry, F.Zhang, G.A.Woolley. *Angew. Chem., Int. Ed.*, **48**, 1484 (2009)
94. L.Stricker, M.Böckmann, T.M.Kirse, N.L.Doltsinis, B.J.Ravoo. *Chem. – Eur. J.*, **24**, 8639 (2018)
95. W.G.Levine. *Drug Metab. Rev.*, **23**, 253 (1991)
96. T.Eom, W.Yoo, S.Kim, A.Khan. *Biomaterials*, **185**, 333 (2018)
97. J.R.Fouts, J.J.Kamm, B.B.Brodie. *J. Pharmacol. Exp. Ther.*, **120**, 291 (1957)
98. M.Staniszewska, S.Kupfer, M.Łabuda, J.Guthmuller. *J. Chem. Theory Comput.*, **13**, 1263 (2017)
99. D.Jacquemin, E.A.Perpète, G.E.Scuseria, I.Ciofini, C.Adamo. *Chem. Phys. Lett.*, **465**, 226 (2008)
100. D.Escudero, S.Trupp, B.Bussemer, G.J.Mohr, L.González. *J. Chem. Theory Comput.*, **7**, 1062 (2011)
101. D.Jacquemin, J.Preat, E.A.Perpète, D.P.Vercauteren, J.M.André, I.Ciofini, C.Adamo. *Int. J. Quantum Chem.*, **111**, 4224 (2011)
102. T.De Meyer, K.Hemelsoet, L.Van der Schueren, E.Pauwels, K.De Clerck, V.Van Speybroeck. *Chem. – Eur. J.*, **18**, 8120 (2012)
103. K.Khayer, T Haque. *ACS Omega*, **5**, 4507 (2020)
104. Y.-S.Lin, G.-D.Li, S.-P.Mao, J.-D.Chai. *J. Chem. Theory Comput.*, **9**, 263 (2013)
105. J.Calbo, C.E.Weston, A.J.White, H.S.Rzepa, J.Contreras-García, M.J.Fuchter. *J. Am. Chem. Soc.*, **139**, 1261 (2017)
106. K.B.Wiberg. *Tetrahedron*, **24**, 1083 (1968)
107. A.R.Thawani, R.-R.Griffiths, A.Jamasb, A.Bourached, P.Jones, W.McCorkindale, A.A.Aldrick, A.A.Lee. *arXiv*, 3226 (2020)
108. W.Sokalski, R.Gora, W.Bartkowiak, P.Kobyliński, J.Sworakowski, A.Chyla, J.Leszczyński. *J. Chem. Phys.*, **114**, 5504 (2001)
109. C.Rietze, E.Titov, S.Lindner, P.Saalfrank. *J. Phys. Condens. Matter*, **29**, 314002 (2017)
110. M.Sumita, M.N.Ryazantsev, K.Saito. *Phys. Chem. Chem. Phys.*, **11**, 6406 (2009)
111. M.N.Ryazantsev, A.Jamal, S.Maeda, K.Morokuma. *Phys. Chem. Chem. Phys.*, **17**, 27789 (2015)
112. D.S.Parker, B.B.Dangi, R.I.Kaiser, A.Jamal, M.Ryazantsev, K.Morokuma. *J. Phys. Chem. A*, **118**, 12111 (2014)
113. J.de Azevedo, F.Walter, R.Dias. *Curr. Drug Targets*, **9**, 1031 (2008)
114. M.D.Parenti, G.Rastelli. *Biotechnol. Adv.*, **30**, 244 (2012)
115. M.V.Westphal, M.A.Schafroth, R.C.Sarott, M.A.Imhof, C.P.Bold, P.Leippe, A.Dhopeshwarkar, J.M.Grandner, V.Katritch, K.Mackie. *J. Am. Chem. Soc.*, **139**, 18206 (2017)
116. G.Cabré, A.Garrido-Charles, A.N.González-Lafont, W.Moormann, D.Langbehn, D.Egea, J.M.Lluch, R.Herges, R.Alibés, F.L.Busqué. *Org. Lett.*, **21**, 3780 (2019)
117. D.Wutz, D.Gluhacevic, A.Chakrabarti, K.Schmidtkunz, D.Robaa, F.Erdmann, C.Romier, W.Sippl, M.Jung, B.König. *Org. Biomol. Chem.*, **15**, 4882 (2017)
118. J.Michel, N.Foloppe, J.W.Essex. *Mol. Inform.*, **29**, 570 (2010)
119. A.de Ruiter, C.Oostenbrink. *Curr. Opin. Struct. Biol.*, **61**, 207 (2020)
120. Z.Cournia, B.Allen, W.Sherman. *J. Chem. Inf. Model.*, **57**, 2911 (2017)
121. I.Cabeza de Vaca, Y.Qian, J.Z.Vilseck, J.Tirado-Rives, W.L.Jorgensen. *J. Chem. Theory Comput.*, **14**, 3279 (2018)
122. S.C.Gill, N.M.Lim, P.B.Grinaway, A.S.Rustenburg, J.Fass, G.A.Ross, J.D.Chodera, D.L.Mobley. *J. Phys. Chem. B*, **122**, 5579 (2018)
123. S.Genheden, U.Ryde. *Expert Opin. Drug Discov.*, **10**, 449 (2015)
124. E.Wang, H.Sun, J.Wang, Z.Wang, H.Liu, J.Z.Zhang, T.Hou. *Chem. Rev.*, **119**, 9478 (2019)
125. N.Homeyer, F.Stoll, A.Hillisch, H.Gohlke. *J. Chem. Theory Comput.*, **10**, 3331 (2014)

126. K.Day, J.D.Schneible, A.T.Young, V.A.Pozdin, L.Gaffney, R.Prodromou, D.Freytes, M.Daniele, S.Menegatti. *J. Mater. Chem. B*, **8**, 33 (2020)
127. D.L.Mobley, M.K.Gilson. *Annu. Rev. Biophys.*, **46**, 531 (2017)
128. V.Kairys, L.Baranauskiene, M.Kazlauskiene, D.Matulis, E.Kazlauskas. *Expert Opin. Drug Discov.*, **14**, 755 (2019)
129. W.D.Cornell, P.Cieplak, C.I.Bayly, I.R.Gould, K.M.Merz, D.M.Ferguson, D.C.Spellmeyer, T.Fox, J.W.Caldwell, P.A.Kollman. *J. Am. Chem. Soc.*, **117**, 5179 (1995)
130. K.Vanommeslaeghe, E.Hatcher, C.Acharya, S.Kundu, S.Zhong, J.Shim, E.Darian, O.Guvench, P.Lopes, I.Vorobyov. *J. Comput. Chem.*, **31**, 671 (2010)
131. U.Ryde, P.Soderhjelm. *Chem. Rev.*, **116**, 5520 (2016)
132. R.Rathore, M.Sumakanth, M.S.Reddy, P.Reddanna, A.A.Rao, M.D.Erion, M.Reddy. *Curr. Pharm. Des.*, **19**, 4674 (2013)
133. F.Fracchia, G.Del Frate, G.Mancini, W.Rocchia, V.Barone. *J. Chem. Theory Comput.*, **14**, 255 (2017)
134. Y.Li, H.Li, F.C.Pickard IV, B.Narayanan, F.G.Sen, M.K.Chan, S.K.Sankaranarayanan, B.R.Brooks, B.Roux. *J. Chem. Theory Comput.*, **13**, 4492 (2017)
135. D.M.Nikolaev, A.A.Shtyrov, M.S.Panov, A.Jamal, O.B.Chakchir, V.A.Kochemirovsky, M.Olivucci, M.N.Ryazantsev. *ACS Omega*, **3**, 7555 (2018)
136. J.Yang, Y.Zhang. *Nucleic Acids Res.*, **43**, W174 (2015)
137. Y.E.Zevatskii, D.Samoilov. *Russ. J. Org. Chem.*, **47**, 1445 (2011)
138. *Computational Approaches for the Prediction of pKa Values*. (Eds G.C.Shields, P.G.Seybold). (Boca Raton, FL: CRC Press, 2013)
139. D.Reis, M.Machuqueiro, D.Vila-Viçosa. In *Proceedings of MOL2NET 2018, International Conference on Multidisciplinary Sciences*. (4th Edn.). 2018. P. 37
140. B.K.Radak, C.Chipot, D.Suh, S.Jo, W.Jiang, J.C.Phillips, K.Schulten, B.Roux. *J. Chem. Theory Comput.*, **13**, 5933 (2017)
141. C.Poornima, P.Dean. *J. Comput. Aided Mol. Des.*, **9**, 521 (1995)
142. S.E.Wong, F.C.Lightstone. *Expert Opin. Drug Discov.*, **6**, 65 (2011)
143. J.Wahl, M.Smieško. *J. Chem. Inf. Model.*, **59**, 754 (2019)
144. O.Carugo, D.Bordo. *Acta Crystallogr., Sect. D: Biol. Crystallogr.*, **55**, 479 (1999)
145. M.Levitt, B.H.Park. *Structure*, **1**, 223 (1993)
146. A.Morozenko, A.Stuchebrukhov. *Proteins*, **84**, 1347 (2016)
147. A.Sridhar, G.A.Ross, P.C.Biggin. *PloS one*, **12**, e0172743 (2017)
148. D.M.Nikolaev, A.A.Shtyrov, A.S.Mereshchenko, M.S.Panov, Y.S.Tveryanovich, M.N.Ryazantsev. *Phys. Chem. Chem. Phys.*, **22**, 18114 (2020)
149. A.Mourot, M.A.Kienzler, M.R.Banghart, T.Fehrentz, F.M.Huber, M.Stein, R.H.Kramer, D.Trauner. *ACS Chem. Neurosci.*, **2**, 536 (2011)
150. D.L.Fortin, M.R.Banghart, T.W.Dunn, K.Borges, D.A.Wagenaar, Q.Gaudry, M.H.Karakossian, T.S.Otis, W.B.Kristan, D.Trauner. *Nat. Methods*, **5**, 331 (2008)
151. J.Safari, Z Zarnegar. *RSC Adv.*, **5**, 17738 (2015)
152. B.Priewisch, K.Rück-Braun. *J. Org. Chem.*, **70**, 2350 (2005)
153. G.Maleeva, D.Wutz, K.Rustler, A.Nin-Hill, C.Rovira, E.Petukhova, A.Bautista-Barrufet, A.Gomila-Juaneda, P.Scholze, F.Peiretti. *Br. J. Pharmacol.*, **176**, 2661 (2019)
154. M.Stein, A.Breit, T.Fehrentz, T.Gudermann, D.Trauner. *Angew. Chem., Int. Ed.*, **52**, 9845 (2013)
155. B.G.Gowenlock, G.B.Richter-Addo. *Chem. Rev.*, **104**, 3315 (2004)
156. R.D.Haworth, A.Lapworth. *J. Chem. Soc.*, **119**, 768 (1921)
157. C.Bleasdale, M.K.Ellis, P.B.Farmer, B.T.Golding, K.F.Handley, P.Jones, W.McFarlane. *J. Labelled Compd. Radiopharm.*, **33**, 739 (1993)
158. W.W.Wood, J.A.Wilkin. *Synth. Commun*, **22**, 1683 (1992)
159. M.D.Johnson, B.J.Hornstein. *Inorg. Chem.*, **42**, 6923 (2003)
160. E.Merino. *Chem. Soc. Rev.*, **40**, 3835 (2011)
161. M.Fetizon, M.Golfier, R.Milcent, I.Papadakis. *Tetrahedron*, **31**, 165 (1975)
162. B.Ortiz, P.Villanueva, F.Walls. *J. Org. Chem.*, **37**, 2748 (1972)
163. H.Firouzabadi, B.Vessal, M.Naderi. *Tetrahedron Lett.*, **23**, 1847 (1982)
164. E.Baer, A.L.Tosoni. *J. Am. Chem. Soc.*, **78**, 2857 (1956)
165. K.Pausacker. *J. Chem. Soc.*, 107 (1953)
166. G.Hughes, B.Saunders. *J. Chem. Soc.*, 4630 (1954)
167. F.Hamon, F.Djedaini-Pilard, F.Barbot, C.Len. *Tetrahedron*, **65**, 10105 (2009)
168. A.A.John, Q.Lin. *J. Org. Chem.*, **82**, 9873 (2017)
169. R.F.Nystrom, W.G.Brown. *J. Am. Chem. Soc.*, **70**, 3738 (1948)
170. R.O.Hutchins, D.W.Lamson, L.Rua, C.Milewski, B.Maryanoff. *J. Org. Chem.*, **36**, 803 (1971)
171. A.Khan, S.Hecht. *Chem. – Eur. J.*, **12**, 4764 (2006)
172. P.S.Mukherjee, N.Das, Y.K.Kryschenko, A.M.Arif, P.J.Stang. *J. Am. Chem. Soc.*, **126**, 2464 (2004)
173. K.Nozawa-Kumada, E.Abe, S.Ito, M.Shigeno, Y.Kondo. *Org. Biomol. Chem.*, **16**, 3095 (2018)
174. M.Cygler, M.Przybylska, R.M.Elofson. *Can. J. Chem.*, **60**, 2852 (1982)
175. C.Galli. *Chem. Rev.*, **88**, 765 (1988)
176. T.I.Godovikova, O.A.Rakitin, L.I.Khmel'nitskii. *Russ. Chem. Rev.*, **52**, 440 (1983)
177. M.Barbero, M.Crisma, I.Degani, R.Fochi, P.Perracino. *Synthesis*, **1998**, 1171 (1998)
178. M.Barbero, I.Degani, S.Dughera, R.Fochi. *J. Org. Chem.*, **64**, 3448 (1999)
179. V.D.Filimonov, M.Trusova, P.Postnikov, E.A.Krasnokutskaya, Y.M.Lee, H.Y.Hwang, H.Kim, K.-W.Chi. *Org. Lett.*, **10**, 3961 (2008)
180. M.J.Hansen, M.M.Lerch, W.Szymanski, B.L.Feringa. *Angew. Chem., Int. Ed.*, **55**, 13514 (2016)
181. Y.-K.Lim, K.-S.Lee, C.-G.Cho. *Org. Lett.* **5**, 979 (2003)
182. D.M.Barber, S.-A.Liu, K.Gottschling, M.Sumser, M.Hollmann, D.Trauner. *Chem. Sci.*, **8**, 611 (2017)
183. D.B.Kimball, M.M.Haley. *Angew. Chem., Int. Ed.*, **41**, 3338 (2002)
184. Y.Zhang, Y.Liu, Xiaogian Ma, Xia Ma, B.Wang, H.Li, Y.Huang, C.Liu. *Dyes Pigm.*, **158**, 438 (2018)
185. L.I.Smith, W.B.Irwin. *J. Am. Chem. Soc.*, **63**, 1036 (1941)
186. W.W.Paudler, A.G.Zeiler. *J. Org. Chem.*, **34**, 3237 (1969)
187. S.Samanta, C.Qin, A.J.Lough, G.A.Woolley. *Angew. Chem., Int. Ed.*, **51**, 6452 (2012)
188. M.Schehr, D.Hugenbusch, T.Moje, C.Näther, R.Herges. *Beilstein J. Org. Chem.*, **14**, 2799 (2018)
189. Y.Fu, M.J.Romero, A.Habtemariam, M.E.Snowden, L.Song, G.J.Clarkson, B.Qamar, A.M.Pizarro, P.R.Unwin, P.J.Sadler. *Chem. Sci.*, **3**, 2485 (2012)

190. K.I.Bártovaá, L.Čechová, E.K.Procházková, O.Socha, Z.Janeba, M.Dracinsky. *J. Org. Chem.*, **82**, 10350 (2017)
191. L.Čechová, J.Filo, M.Dračínský, C.Slavov, D.Sun, Z.Janeba, T.Slanina, J.Wachtveitl, E.Procházková, M.Cigá. *Angew. Chem., Int. Ed.*, **59**, 15590 (2020); https://doi.org/10.1002/anie.202007065
192. J.Balam-Villarreal, B.López-Mayorga, D.Gallardo-Rosas, R.Toscano, M.Carreón-Castro, V.Basiuk, F.Cortés-Guzmán, J.López-Cortés, M.Ortega-Alfaro. *Org. Biomol. Chem.*, **18**, 1657 (2020)
193. Y.Li, B.O.Patrick, D.Dolphin. *J. Org. Chem.*, **74**, 5237 (2009)
194. C.Lin, L.Yang, M.Xu, Q.An, Z.Xiang, X.Liu. *RSC Adv.*, **6**, 51552 (2016)
195. J.A.Mondal, G.Saha, C.Sinha, D.K.Palit. *Phys. Chem. Chem. Phys.*, **14**, 13027 (2012)
196. D.Banerjee, U.Ray, S.Jasimuddin, J.-C.Liou, T.-H.Lu, C.Sinha. *Polyhedron*, **25**, 1299 (2006)
197. G.Saha, P.Datta, K.K.Sarkar, R.Saha, G.Mostafa, C.Sinha. *Polyhedron*, **30**, 614 (2011)
198. G.Crank, B.Mekonnen. *J. Heterocycl. Chem.*, **29**, 1469 (1992)
199. S.Kolodyazhnaya, L.Divaeva, R.Sogomonova, A.Simonov. *Chem. Heterocycl. Compd.*, **26**, 538 (1990)
200. M.M.M.Raposo, A.M.Ferreira, M.Amaro, M.Belsley, J.C.Moura. *Dyes Pigm.*, **83**, 59 (2009)
201. S.Ogasawara, S.Ito, H.Miyasaka, M.Maeda. *Chem. Lett.*, **39**, 956 (2010)
202. R.Zhu, R.P.Baumann, P.G.Penketh, K.Shyam, A.C.Sartorelli. *J. Med. Chem.*, **56**, 1355 (2013)
203. T.M.Klapötke, D.G.Piercey. *Inorg. Chem.*, **50**, 2732 (2011)
204. B.Jiang, Y.Ning, W.Fan, S.-J.Tu, G.Li. *J. Org. Chem.*, **79**, 4018 (2014)
205. C.Schütt, G.Heitmann, T.Wendler, B.Krahwinkel, R.Herges. *J. Org. Chem.*, **81**, 1206 (2016)
206. Y.Xu, C.Gao, J.Andréasson, M.Grøtli. *Org. Lett.*, **20**, 4875 (2018)
207. D.A.Kolarski, W.Szymanski, B.L.Feringa. *Org. Lett.*, **19**, 5090 (2017)
208. P.Kumar, A.Srivastava, C.Sah, S.Devi, S.Venkataramani. *Chem. – Eur. J.*, **25**, 11924 (2019)
209. L.Stricker, E.-C.Fritz, M.Peterlechner, N.L.Doltsinis, B.J.Ravoo. *J. Am. Chem. Soc.*, **138**, 4547 (2016)
210. C.E.Weston, A.Krämer, F.Colin, O.Z.Yildiz, M.G.Baud, F.-J.Meyer-Almes, M.J.Fuchter. *ACS Infect. Dis.*, **3**, 152 (2017)
211. P.M.Pithan, C.Kuhlmann, C.Engelhard, H.Ihmels. *Chem. – Eur. J.*, **25**, 16088 (2019)
212. R.Travieso-Puente, S.Budzak, J.Chen, P.Stacko, J.T.Jastrzebski, D.Jacquemin, E.Otten. *J. Am. Chem. Soc.*, **139**, 3328 (2017)